Construction of a fluorescent biosensor family

ROBERT M. DE LORIMIER, J. JEFF SMITH, MARY A. DWYER, LOREN L. LOOGER, KEVIN M. SALI, CHAD D. PAAVOLA,[1] SHAHIR S. RIZK, SHAMIL SADIGOV, DAVID W. CONRAD, LESLIE LOEW,[2] AND HOMME W. HELLINGA[3]

Department of Biochemistry, Duke University Medical Center, Durham, North Carolina 27710, USA
[1]Astrobiology Technology Branch, NASA Ames Research Center, Moffett Field, California 94035, USA
[2]Center for Biomedical Imaging Technology and Department of Physiology, University of Connecticut Health Center, Farmington, Connecticut 06030, USA

(RECEIVED June 7, 2002; FINAL REVISION August 16, 2002; ACCEPTED August 22, 2002)

Abstract

Bacterial periplasmic binding proteins (bPBPs) are specific for a wide variety of small molecule ligands. bPBPs undergo a large, ligand-mediated conformational change that can be linked to reporter functions to monitor ligand concentrations. This mechanism provides the basis of a general system for engineering families of reagentless biosensors that share a common physical signal transduction functionality and detect many different analytes. We demonstrate the facility of designing optical biosensors based on fluorophore conjugates using 8 environmentally sensitive fluorophores and 11 bPBPs specific for diverse ligands, including sugars, amino acids, anions, cations, and dipeptides. Construction of reagentless fluorescent biosensors relies on identification of sites that undergo a local conformational change in concert with the global, ligand-mediated hinge-bending motion. Construction of cysteine mutations at these locations then permits site-specific coupling of environmentally sensitive fluorophores that report ligand binding as changes in fluorescence intensity. For 10 of the bPBPs presented in this study, the three-dimensional receptor structure was used to predict the location of reporter sites. In one case, a bPBP sensor specific for glutamic and aspartic acid was designed starting from genome sequence information and illustrates the potential for discovering novel binding functions in the microbial genosphere using bioinformatics.

Keywords: Periplasmic binding proteins; biosensor; conformational change; fluorescence, ratiometry; bioinformatics

Biosensors are analytical tools that measure the presence of a single molecular species in complex mixtures by combining the exquisite molecular recognition properties of biological macromolecules with signal transduction mechanisms that couple ligand binding to readily detectable physical changes (Hall 1991; Scheller et al. 2001). Ideally, a biosensor is reagentless and does not change composition as a consequence of making the measurement (Hellinga and Marvin 1998), unlike enzyme-based assays or competitive immunoassays, for instance. Most biosensors combine a naturally occurring macromolecule such as an enzyme or an antibody, with the identification of a suitable physical signal particular to the molecule in question, and the construction of a detector specific to that system (Meadows 1996). Recently, molecular engineering techniques have been explored to develop macromolecules that combine a wide range of binding specificities and affinities with a common signal transduction mechanism, to construct a generic detection system for many different analytes (Hellinga and Marvin 1998). Here we demonstrate that protein engineering techniques, based on straightforward structural prin-

[3]Reprint requests to: Homme Hellinga, Department of Biochemistry, Box 3711, Duke University Medical Center, Durham, NC 27710; e-mail: hwh@biochem.duke.edu; fax (919) 684-8885.

Abbreviations: BP, binding protein; bPBP, bacterial periplasmic binding protein; PCR, polymerase chain reaction; ΔI_{std}, standard intensity change; ΔR, standard ratiometric change; ΔR_{max}, maximum value of standard ratiometric change; F, fluorescence intensity; F_F, fluorescence intensity in ligand-free state; F_B, fluorescence intensity in ligand-saturated state; S, ligand concentration; R, fluorescence ratio; R_F, fluorescence ratio in ligand-free state; R_B, fluorescence ratio in ligand-saturated state; MOPS, 3-morpholinopropanesulfonic acid; NBD, N,N'-dimethyl-N-(iodoacetyl)-N'-(7-nitrobenz-2-oxa-1,3-diazol-4-yl)ethylenediamine; NBDE, N-[2–(iodoacetoxy-ethyl]-N-methyl)amino-7-nitrobenz-2-oxa-1,3-diazole

Article and publication are at http://www.proteinscience.org/cgi/doi/10.1110/ps.021860.

ciples, can be used systematically to adapt the bacterial periplasmic binding proteins (bPBPs) into a versatile biosensor system that combines the large, natural ligand-binding diversity found within this superfamily with generic, reagentless, engineered signal transduction mechanisms. We demonstrate that the biodiversity of this superfamily can be readily exploited to generate biosensors for a wide variety of chemical classes with widespread potential utility (Table 1), including sugars, amino acids, dipeptides, cations, and anions.

Escherichia coli bPBPs are members of a protein superfamily (Tam and Saier Jr. 1993) that is proving to be well suited for the engineering of biosensors. These proteins consist of two domains linked by a hinge region (Quiocho and Ledvina 1996). The ligand-binding site is located at the interface between the two domains. The proteins typically adopt two conformations: a ligand-free open form and a liganded closed form, which interconvert via a hinge-bending mechanism upon ligand binding. This global, ligand-mediated conformational change has been exploited to couple ligand binding to changes in fluorescence intensity by positioning single, environmentally sensitive fluorophores in locations that undergo local conformational changes in concert with the global change (Brune et al. 1994; Gilardi et al. 1994, 1997; Marvin et al. 1997; Marvin and Hellinga 1998, 2001a; Tolosa et al. 1999; Dattelbaum and Lakowicz 2001; Salins et al. 2001). Conformational coupling mechanisms can also be devised to alter the flow of current between the surface of an electrode derivatized with the engineered bPBP containing a covalently attached redox cofactor (Benson et al. 2001). These engineered conformational coupling mechanisms allow reagentless optical and electrochemical biosensors to be constructed using the bPBPs.

The engineered conformational coupling mechanisms are universal to all bPBPs that undergo a ligand-mediated hinge-bending motion and should therefore permit modular manipulation of ligand-binding specificity and affinity, as the reporter group and ligand-binding sites can be sterically separated (Marvin et al. 1997; Marvin and Hellinga 1998). Using engineered maltose-binding protein (maltose BP), we have previously demonstrated that specificity can be radically changed without destroying the reagentless optical (Marvin and Hellinga 2001a) or electrochemical (Benson et al. 2001) signal transduction mechanism. Similarly the ligand-binding affinity can be drastically altered in maltose BP with retention of the conformational coupling mechanism (Marvin et al. 1997; Marvin and Hellinga 2001a). Here we present an investigation into the universality of the engineered conformational coupling mechanism. We have used 10 bPBPs of known structure and introduced 8 different environmentally sensitive fluorophores at a variety of locations predicted to link local conformational changes to the global, ligand-mediated hinge-bending motion. Furthermore, we show that bioinformatics techniques can be used to predict the location of linked sites in bPBPs whose structure is not known, thereby opening opportunities for using the large number of paralogs and homologs that have recently been identified in this family by genomic sequencing studies (Blattner et al. 1997; Quentin et al. 1999). Together with the opportunities of structure-based redesign of ligand-binding specificity (Hellinga and Richards 1991; Marvin and Hellinga 2001a; M.A. Dwyer, L.L. Looger, J.J. Smith, and H.W. Hellinga, unpubl.; L.L. Looger, M.A. Dwyer, J.J. Smith, and H.W. Hellinga, unpubl.), these studies demonstrate the vast potential of the bPBP superfamily as the basis for a system of biosensors suited to a broad range of applications.

Table 1. *Potential applications of biosensors for bPBP ligands*

	Application		
Analyte	Clinical	Industrial	Environmental
arabinose		Deanda et al. 1996	
glucose	Burrin and Price 1985	AOAC 1995	
maltose	Nelson et al. 1977	AOAC 1995	
ribose		AOAC 1995	
glutamate	Burtis and Ashwood 1994	AOAC 1995	
glutamine	Smith and Forman 1994		
histidine	Taylor et al. 1991		
dipeptides			
phosphate	Burkhardt et al. 1979		APHA 1992
sulfate			EPA 1999
Fe(III)			Martin 1992

Results

Family of biosensors

A set of 11 bPBPs with widely varying ligand-binding specificities was selected for engineering biosensor function (Table 2). All were from *E. coli* except Fe(III) BP, which is from *Haemophilus influenzae*. Binding specificities and affinities of these proteins for their respective ligands have been characterized (references in Table 2). Three proteins bind monosaccharides (arabinose, glucose, and ribose BP), one binds di- and trisaccharides of glucose (maltose BP), three bind amino acids (glutamate/aspartate, histidine, and glutamine BP), one binds di- and tripeptides (dipeptide BP), two bind oxyanions (phosphate and sulfate BP), and one binds a metal ion [Fe(III) BP]. Most of these bPBPs bind at most two or three related ligands with high affinity (micromolar or better). For example, phosphate BP binds phosphate and arsenate but not other oxyanions (Luecke and Quiocho 1990), and glucose BP binds glucose and galactose but not other monosaccharides (Anraku 1968). Dipeptide BP is an exception in that it binds a wide variety of di- and

Table 2. *References and PDB[a] files for bPBP structures, genes, and ligand binding*

	Crystal structure			
bBPB	Open form	Closed form	DNA sequence	Ligand affinity
arabinose BP		Quiocho and Vyas 1984 1ABE	Scripture et al. 1987	Clark et al. 1982; Miller III et al. 1983
dipeptide BP	Nickitenko et al. 1995 1DPE	Dunten and Mowbray 1995 1DPP	Abouhamad et al. 1991	Guyer et al. 1986; Smith et al. 1999
Glu/Asp BP				Barash and Halpern 1975; Willis and Furlong 1975
Fe(III) BP	Bruns et al. 2001 1D9V	Bruns et al. 1997 1MRP	Sanders et al. 1994	Adhikari et al. 1995
glucose BP		Vyas et al. 1988; Vyas et al. 1994 1GLG	Scholle et al. 1987	Anraku 1968
histidine BP		Yao et al. 1994 1HSL	Joshi and Ames 1996[b]	Miller III et al. 1983
maltose BP	Sharff et al. 1992 1OMP	Spurlino et al. 1991; Quiocho et al. 1997 1ANF	Duplay et al. 1984	Schwartz et al. 1976
phosphate BP	Ledvina et al. 1996. 1OIB	Luecke and Quiocho 1990 1IXH	Magota et al. 1984	Medveczky and Rosenberg 1969
glutamine BP	Hsiao et al. 1996 1GGG	Sun et al. 1998 1WDN	Nohno et al. 1986	Weiner et al. 1971
ribose BP	Bjorkman and Mowbray 1998	Mowbray and Cole 1992 2DRI	Groarke et al. 1983	Willis and Furlong 1974
sulfate BP		Pflugrath and Quiocho 1985; He and Quiocho 1993 1SBP	Hellinga and Evans 1985	Jacobson and Quiocho 1988

[a]Protein Data Bank (Berman et al. 2000).
[b]GenBank Accession No. U47027.

tripeptides (Smith et al. 1999). Measured ligand dissociation constants in these proteins are typically in the range of 0.1–1 μM. An exception is Fe(III) BP, where the K_d for $Fe(III)_{(aq)}$ is estimated to be 10^{-21} M in competition assays with Fe(III) chelates (Adhikari et al. 1995).

For 9 of the 11 proteins selected for this study crystal structures have been solved of the closed, ligand-bound state (Table 2). In the case of sulfate BP, the crystal structure of the *E. coli* protein has not been reported, so that of *Salmonella typhimurium* sulfate BP was adopted to model the *E. coli* protein. Sulfate BP from *E. coli* and *S. typhimurium* are 95% identical in amino acid sequence and hence likely to have highly similar structures, in analogy to histidine BP from these two organisms (Oh et al. 1994; Yao et al. 1994). Structures have been solved for the open unliganded state for 6 of the 11 proteins as well (Table 2).

Structure-based design of conformational coupling

Linkage between ligand binding and change in fluorescence of a covalently coupled environmentally sensitive fluorophore can be established if the local environment of the fluorophore changes in concert with formation of the complex. Two mechanisms can be distinguished to establish such structural linkage relationships. Direct linkage involves formation of a nonbonded contact between the bound ligand and the conjugated fluorophore. Indirect linkage involves changes in the local protein structure in the immediate vicinity of the attached fluorophore, and relies on ligand-mediated conformational changes such as the hinge-bending motion observed in the bPBPs.

Direct linkage relationships are readily designed by replacing a residue known to form a ligand contact with a cysteine to which the fluorophore is attached ("endosteric" attachment site). Indirect linkage relationships can be established in two ways. The most straightforward method relies on visual inspection of the ligand complex structure and identifying residues that are located in the vicinity of the binding site but do not interact directly with the ligand and that are likely to be involved in conformational changes. In the case of the bPBPs such are residues located at the perimeter of the interdomain cleft that forms the ligand binding site. The environment of these "peristeric" sites changes significantly upon formation of the closed state. The second approach identifies sites in the protein structure that are located some distance away from the ligand-binding site and undergo a local conformational change in concert with ligand binding. If the structures of both the open and closed states are known, then such "allosteric" sites can be identified using a computational method that analyzes the conformational change (Marvin et al. 1997). Alternatively, once allosteric sites have been identified in one bPBP, structural homology arguments can be invoked to identify such sites in other bPBPs in which only one state has been characterized (Marvin and Hellinga 1998). Table 3 summarizes the designs of all three classes of sites in each of the receptors used in this study. The locations of these sites in the 11 bPBPs are shown in Figure 1.

Sequence-based design of conformational coupling

The number of bPBPs of known sequence greatly exceeds the number for which structures have been solved or for

Table 3. *Fluorophore conjugation sites*

Protein	Mutant	Steric category[a]	Design method[b]	Protein	Mutant	Steric category[a]	Design method[b]
arabinose BP	D275C	a	3	histidine BP	E167C	p	1
	F23C	a	3		K229C	p	1
	K301C	a	3		V163C	p	1
	L253C	a	3		Y230C	p	1
	L298C	a	3		F231C	p	1
dipeptide BP	D450C	p	1		Y88C	a	3
	K394C	p	1	maltose BZP	D95C	a	2
	R141C	p	1		F92C	a	2
	S111C	p	1		I329C	a	2
	T44C	p	1		S233C	p	2
	W315C	p	1	phosphate BP	A225C	a	2
Glu/Asp BP	A207C	p	4		N223C	a	2
	A210C	p	4		N226C	a	2
	E119C	p	4		S164C	p	2
	F126C	a	4		S39C	p	2
	F131C	a	4	glutamine BP	N160C	p	2
	F270C	p	4		F221C	p	2
	G211C	p	4		K219C	p	2
	K268C	p	4		L162C	p	2
	Q123C	p	4		W220C	p	2
	T129C	a	4		Y163C	p	2
Fe(III) BP	E203C	p	1		Y86C	a	2
	K202C	p	1	ribose BP	T135C	p	2
	K85C	a	1		D165C	p	2
	V287C	a	1	E192	C	p	2
glucose BP	Y10C	e	1		A234C	a	2
	N15C	p	1		L236C	a	2
	E93C	p	1		L265C	a	2
	E149C	p	1	sulfate BP	L65C	p	1
	H152C	e	1		N70C	p	1
	W183C	e	1		Q294C	p	1
	L255C	a	3		R134C	p	1
	D257C	a	3		W290C	p	1
	V296C	a	3		Y67C	p	1

[a] (a) Allosteric; (e) endosteric; (p) peristeric.
[b] (1) Visual inspection of the closed structure; (2) identification by automated comparison of the open and closed states; (3) structural homology; (4) sequence homology.

which functions have been assigned by genetic or biochemical characterization. To exploit this reservoir of potential biosensors, coding sequences for bPBPs must be identified and their putative ligand-binding specificities must be established. The identification of bPBPs in microbial genomes relies on finding amino acid sequence homologies to particular clusters of the bPBP family (Tam and Saier 1993). Ligand-binding can then be determined by direct experimentation or be inferred either by structural relationships to bPBPs of known function or by establishing genetic linkage to other genes of known function (Pellegrini et al. 1999). Subsequently, sites within the homolog that undergo local conformational change, and to which reporter functions can be attached, must be identified. The selection of sites for attaching reporter functions relies on homology to bPBPs of known structure.

To illustrate these principles we sought to construct a glutamate biosensor starting from genome sequence data only. The genome of *E. coli* K12 contains the locus *ybeJ* encoding a protein identified as a putative bPBP based on amino acid sequence homology with glutamine and histidine BPs (26% and 23% sequence identity; 41% and 43% sequence similarity, respectively) (Blattner et al. 1997). The assignment of YBEJ as an amino acid-binding protein was strengthened by the presence of conserved residues found to be associated with binding to the α-amino and α-carboxylate groups of the ligand in all bPBP amino acid-binding proteins of known structure identified in *E. coli* (Table 4). Of additional interest is the presence of an arginine residue in YBEJ located at a position that in the other amino acid-binding proteins interacts directly with the side chain of the bound amino acid, suggesting that YBEJ binds an amino

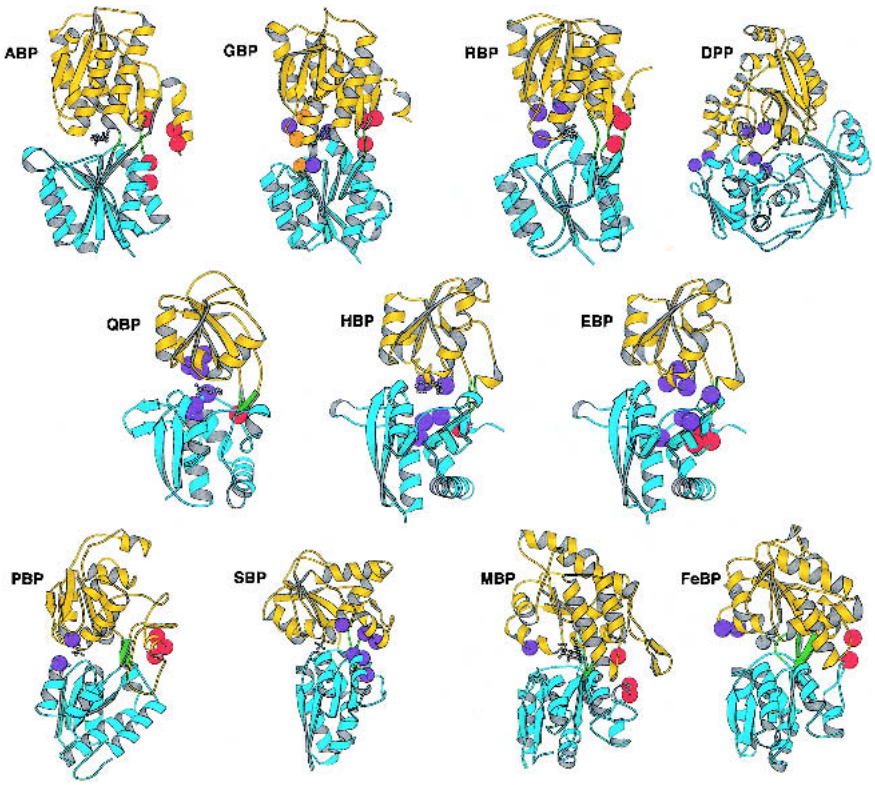

Fig. 1. Structures of 11 bPBPs, indicating locations of allo-, endo-, and peristeric sites used in this study. Each protein is shown in the closed form, with bound ligand indicated by gray ball-and-stick structures. The two domains of each bPBP are differentiated as blue or yellow ribbons, the former containing the N terminus. Hinge segments connecting the domains are green. The structure of histidine BP is used to represent the as-yet-unsolved structure of glutamate/aspartate BP. Residues mutated to cysteine are indicated by colored spheres and differentiated as allosteric (red), endosteric (orange, in GBP only), or peristeric (purple). Structures are grouped by cluster as defined by Tam and Saier Jr. (1993), according to sequence-based relationships. Cluster 2: (ABP) arabinose BP; (GBP) glucose BP; (RBP) ribose BP. Cluster 5: (DPP) dipeptide BP. Cluster 3: (QBP) glutamine BP; (HBP)histidine BP; (EBP) glutamate/aspartate BP. Cluster 6: (PBP) phosphate BP; (SBP) sulfate BP. Cluster 1: (MBP) maltose BP; (FeBP) Fe(III) BP. Molecular graphics were rendered with Molscript (Kraulis 1991).

acid bearing a negatively charged side chain. Finally, *ybeJ* is located adjacent to three tandem genes (*gltJ*, *gltK*, *gltL*) postulated to be involved in the glutamate/aspartate transport system (Lum and Wallace 1995 GenBank Accession No. U10981), suggesting that *ybeJ* encodes a glutamate/aspartate BP. Putative allo-, endo-, and peristeric sites were identified from a structure-based sequence alignment of YBEJ with glutamine BP and histidine BP (Fig. 2).

Mutagenesis and protein production

All of the genes for the bPBPs used in this study were cloned from *E. coli* or *H. influenzae* genomic DNA using PCR. The leader peptide sequence that directs expression into the periplasm was identified by comparison to the known N terminus of the protein, or, in the case of YBEJ, by homology to known leader sequences (von Heijne 1986).

Table 4. *Ligand interactions with residues in polar amino acid binding proteins*

Ligand group[a]	sc	sc	sc	αN	αN	αC	sc	sc	αC	αN
glutamine BP	D10	F13	F50	G68	T70	R75	K115	T118	G119	D157
histidine BP	D11	Y14	L52	S70	S72	R77	L117	T120	T121	D161
lys/arg/orn BP	D11	Y14	F52	S70	S72	R77	L117	T120	T121	D161
YBEJ	R25	S28	S73	S91	T93	R98	T137	T140	T141	D183

[a] (sc) Side chain, (αN) α-amino; (αC) α-carboxy.

```
                          47                  67                  87                 107                 127
gln BP  ----------ADKKLVVATD TAFVPFEFKQGD-KYVGFDV DLWAAIAKELK-------LD YELKPMDFSGIIPALQTKNV DLALAGITITDERKKAIDFS
his BP  ---------AIPQNIRIGTD PTYAPFESKNSQGELVGFDI DLAKELCKRIN-------TQ CTFVENPLDALIPSLKAKKI DAIMSSLSITEKRQQEIAFT
  YBEJ  MAGSTLDKIAKNGVIVVGHR ESSVPFSYYDNQQKVVGYSQ DYSNAIVEAVKKKLNKPDLQ VKLIPITSQNRIPLLQNGTF DFECGSTTNNVERQKQAAFS
                                                                                                  p   p  a

                          147                 166                 186                 206                 226
gln BP  DGYYKSGLLVMVKANNNDVK SVKDLDGKVVAVKSGTGSVD YAKANIKTK--DLRQFPNID N--AYMELGTNRADAVLHDT PNILY-FIKTAGNGQFKAVG
his BP  DKLYAADSRLVVAKNSDIQP TVESLKGKRVGVLQGTTQET FGNEHWAPKGIEIVSYQGQD N--IYSDLTAGRIDAAFQDE VAASEGFLKQPVGKDYKFGG
  YBEJ  DTIFVVGTRLLTKKGGD-IK DFANLKDKAVVVTSGTTSEV LLNKLNEEQKMNMRIISAKD HGDSFRTLESGRAVAFMMDD ALLAGERAKAKKPDNWEIVG
         a a                                                                                  pp pp

                          241                 261                 281                 301
gln BP DSLEAQQYG-----IAFPKG SDELRDKVNGALKTLRENGT YNEIYKKWFGTEPK------ -------------------- -
his BP PSVKDEKLFGVGTGMGLRKE DNELREALNKAFAEMRADGT YEKLAKKYFDFDVYGG---- -------------------- -
  YBEJ KPQSQEAYG-----CMLRKD DPQFKKLMDDTIAQVQTSGE AEKWFDKWFKNPIPPKNLNM NFELSDEMKALFKEPNDKAL N
                                                 ppp
```

Fig. 2. Alignment of sequences of *E. coli* YBEJ (putative glutamate/aspartate BP), glutamine BP, and histidine BP using clustalW (Thompson et al. 1994). Numbering begins from the putative initiation codon of the open reading frame for YBEJ, including its leader sequence. The underlined methionine is the initiation codon for expression of YBEJ used in this study. Residues in each protein that were mutated to cysteine for fluorophore conjugation are in boldface type. (a) Allosteric; (p) peristeric.

The protein was produced by overexpression of the processed form in the cytoplasm with an initiation methionine placed just before the N terminus of the processed protein, under the control of a strong inducible promoter in the pAED4 (Doering 1992), pET-21a (Studier et al. 1990) (Novagen), or pKK223–3 (Brosius and Holy 1984) plasmids. An oligohistidine tag was fused to the C terminus of the cloned receptor to permit facile purification by immobilized metal affinity chromatography (Hochuli et al. 1987). In all cases the receptors expressed well (at least 50 mg of pure protein per liter of fermentation). The molecular masses estimated by gel electrophoresis corresponded to the predicted mass of the expressed reading frame.

Cysteine point mutations were introduced by the PCR overlap method (Ho et al. 1989). Mutant proteins typically expressed as well as the wild-type protein. All cysteine substitutions in arabinose BP were constructed in the C64A background to prevent interference from this endogenous cysteine (Miller III et al. 1979). In the case of Fe(III) BP, all mutations were constructed in the E57D background. In the crystal structure of Fe(III) BP, this glutamate is coordinated to the iron (Bruns et al. 1997). We found that the E57D mutation weakens the affinity of Fe(III) BP for Fe(III) from approximately 1×10^{-21} M (Adhikari et al. 1995) to approximately 3×10^{-8} M, assuming a stability constant for the 1:1 Fe(III) citrate complex of logK = 10.25 (Martell and Smith 1977). This permitted straightforward determination of Fe(III) affinity by direct titration with Fe(III) citrate at nanomolar concentrations of Fe(III) BP.

Signal transduction by fluorescence

To report ligand binding by the set of 11 bPBPs, fluorescent reporter groups were attached to single cysteine thiols engineered into sites that were predicted to undergo binding-dependent conformational change. We examined eight thiol-reactive fluorophores chosen on the basis of the sensitivity of their emission spectra to changes in environment and spanning a wide range of emission and excitation wavelengths (Fig. 3). The results for all biosensor conjugates are presented in Table 5 (11 receptors, 68 cysteine mutants, 320 fluorophore conjugates).

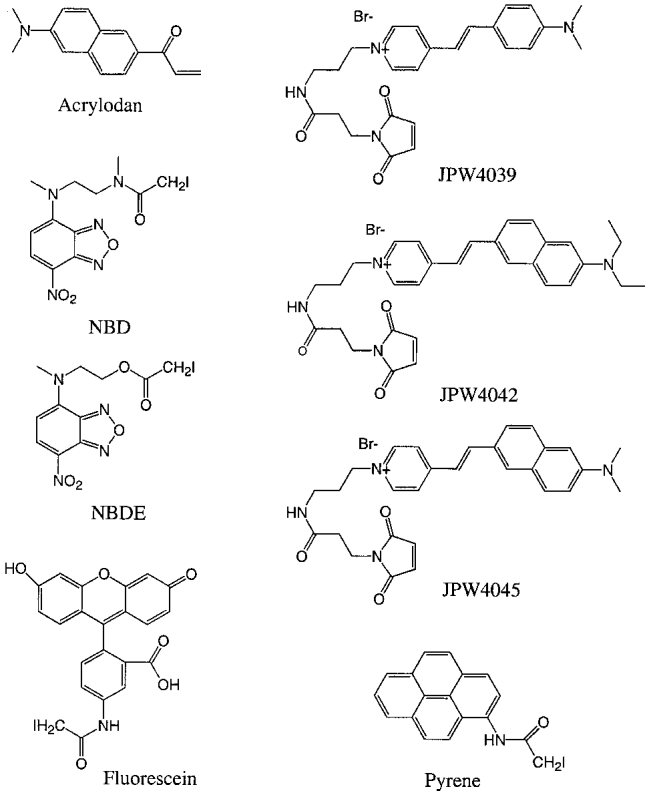

Fig. 3. Structural formulae of thiol-reactive fluorophores. Approximate wavelengths of maximal fluorescence excitation and emission, respectively, of the protein-bound fluorophores are (in nm): pyrene (340, 390); acrylodan (390, 500); fluorescein (485, 520); NBD (490, 540); NBDE (490, 530); JPW4039 (485, 590); JPW4042 (470, 640); and JPW4045 (470, 640).

Assessment of fluorescent biosensor function

Fluorescence emission spectra of bPBP-fluorophore conjugates were recorded in the absence and presence of saturating ligand concentrations. Spectral changes were characterized by four parameters: wavelength shift (the difference between the wavelengths of emission maximum in the unbound and ligand-saturated states), direction of intensity change (increase or decrease in intensity at the wavelengths of maximum emission in the two states), standard intensity change (ΔI_{std}), and standard ratiometric change (ΔR). ΔI_{std} is defined as the normalized intensity change relative to the average intensity, determined at the wavelength midpoint between the two emission maxima:

$$\Delta I_{std} = \left| \frac{2(I_1(\lambda_{std}) - I_2(\lambda_{std}))}{I_1(\lambda_{std}) + I_2(\lambda_{std})} \right| \quad (1)$$

where $\lambda_{std} = (\lambda_{max,\ unbound} + \lambda_{max,\ saturated})/2$ and I_1, I_2 are the fluorescence intensities at λ_{std} of each spectrum respectively (Fig. 4A). ΔR is defined in terms of two emission bands, A_1 ($[\lambda_1, \lambda_2]$) and A_2 ($[\lambda_3, \lambda_4]$) (Fig. 4B):

$$\Delta R = \left| \frac{{}^{0}A_1}{{}^{0}A_2} - \frac{{}^{\infty}A_1}{{}^{\infty}A_2} \right| \quad (2)$$

where ${}^{o}A_1$, ${}^{o}A_2$ are the areas in the absence of ligand, and ${}^{\infty}A_1$, ${}^{\infty}A_2$ are the areas in the presence of saturating ligand. A computer program was used to enumerate ΔR for all possible pairs of wavelength bands in the two spectra, to identify the optimal sensing condition, defined as the maximum value of ΔR. Adjustable parameters of the algorithm, and their values used for ΔR_{max} quantities reported here, are step size (2 nm), step width (10 nm), minimum integration area limit (fraction of total: 0.1), and maximum integration area limit (fraction of total: 1).

Analyte affinity measurements

A total of 133 bPBP-fluorophore conjugates with $\Delta I_{std} > 0.1$ were used to determine ligand binding affinity by fluorimetric titration (Table 5). The emission wavelength monitored was that of maximum difference in intensity between the ligand-free and bound states. For each conjugate fluorescence intensiometric observations were fit to a hyperbolic binding isotherm for a two-state model (Marvin et al. 1997):

$$F = \frac{K_d F_F + [S]F_B}{K_d + [S]} \quad (3)$$

where F is fluorescence at ligand concentration [S], K_d is the dissociation constant, and F_F, F_B are the fluorescence intensities of the ligand-free and ligand-saturated states, respectively. Examples of binding isotherms are shown in Figure 5 for glucose BP and glutamate/aspartate BP. For ratiometric observations, equation 3 has to be modified to account for differentially weighted contributions of the two emission bands (Lakowicz 1999):

$$R = \frac{{}^{app}K_d R_F + [S]R_B}{{}^{app}K_d + [S]} \quad (4)$$

where R is ratio A_1/A_2, $R_B = {}^{\infty}A_1/{}^{\infty}A_2$, $R_F = {}^{0}A_1/{}^{0}A_2$, and ${}^{app}K_d$ is an apparent dissociation constant:

$${}^{app}K_d = \frac{{}^{0}A_2}{{}^{\infty}A_2} K_d \quad (5)$$

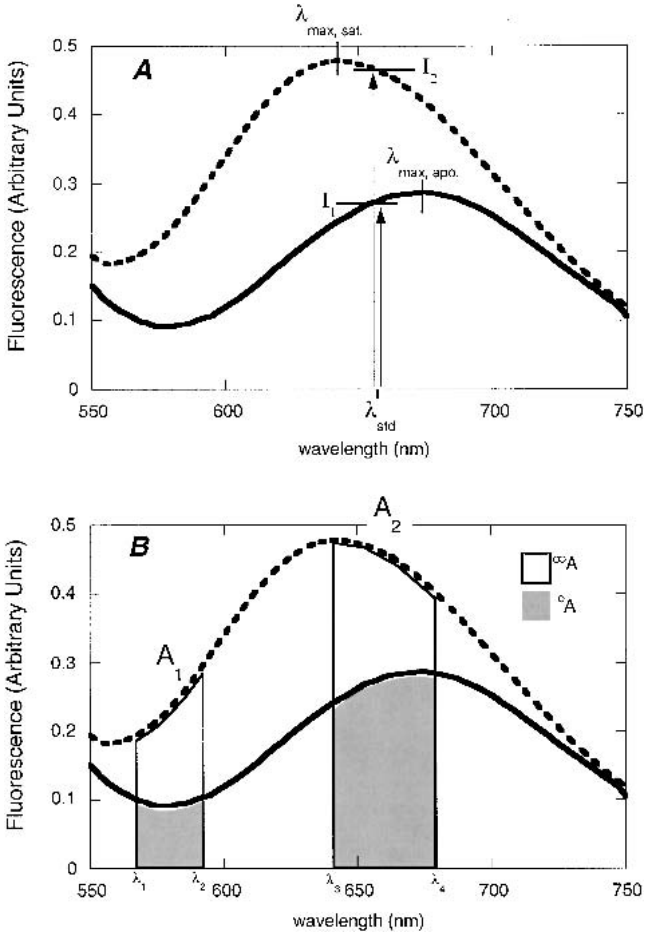

Fig. 4. Definition of fluorimetric parameters. (*A*) Parameters λ_{std}, I_1, and I_2 used to determine the standard intensity change ΔI_{std}. (*B*) Parameters A_1, A_2, ^{o}A, and $^{\infty}A$ used to determine ΔR. Each of the areas $^{\infty}A$ encompasses the respective area ^{o}A.

Table 5. *Spectral and binding parameters of fluorophore-conjugated bPBPs*

Protein[a]	Mutant	Site[b]	Fluorophore	Ligand	$\lambda_{max,\ apo}$	$\lambda_{max,\ sat}$	ΔI_{std}[c]	Inc/dec[d]	ΔR_{max}[c]	K_d (μM)	Std. error
arabinose BP	D257C	a	JPW4039	arabinose	600	596	**0.38**	–	0.92	90	3
			Acrylodan		495	495	**0.26**	–	**1.66**	56	7
			Fluorescein		519	520	0.03	–	1.17	4.0	0.4
			NBD		538	544	0.22	+	1.15	32	2
	F23C	a	JPW4039		587	588	**0.93**	–	0.76	38	1
			Acrylodan		503	503	0.02	+	0.99	3.9	0.6
			Fluorescein		519	519	0.04	–	0.45	3.2	0.5
			NBD		543	548	**0.38**	–	0.76	5.0	0.1
	K301C	a	JPW4039		582	588	**1.20**	–	**1.73**	77	4
			Acrylodan		486	486	0.10	–	1.19	0.46	0.01
			Fluorescein		518	517	**0.41**	+	1.06	24	1
			NBD		532	538	0.08	–	**3.15**	31	1
	L253C	a	JPW4039		590	589	**0.83**	–	**1.31**	165	8
			Acrylodan		482	495	0.05	–	**1.81**	0.69	0.10
			Fluorescein		519	515	0.24	–	**2.71**	48	3
			NBD		539	539	**0.41**	+	**1.66**	775	49
	L298C	a	JPW4039		591	591	**0.42**	–	0.65	70	2
			Acrylodan		499	500	0.07	–	**1.77**	44	2
			Fluorescein		518	518	0.02	–	0.48		
			NBD		543	539	**0.45**	+	0.41	56	4
dipeptide BP	D450C	p	JPW4039	Gly-Leu	602	604	0.20	–	0.29	0.91	0.20
			JPW4042		666	664	0.20	–	1.08	1.5	0.3
			JPW4045		663	666	0.23	–	1.18	2.0	0.5
			Acrylodan		508	521	0.06	+	**1.64**	11	4
			Fluorescein		520	520	0.10	+	0.04		
			NBD		545	544	0.02	–	0.80		
	K394C	p	JPW4039		592	598	**0.37**	+	**1.34**	30	2
			JPW4042		638	644	0.06	+	0.99	78	8
			JPW4045		631	640	0.01	+	1.07		
			Acrylodan		500	500	0.23	+	0.90	23	2
			Fluorescein		522	522	**0.30**	+	0.21	93	6
			NBD		542	541	0.06	–	0.68	0.012	0.005
	R141C	p	JPW4039		592	596	0.06	–	0.69		
			JPW4042		629	631	0.06	–	0.87		
			JPW4045		610	617	0.15	–	1.18		
			Acrylodan		502	501	0.06	–	0.25	2.3	1.2
			Fluorescein		522	522	0.12	–	0.66	38	14
			NBD		542	544	0.00	+	0.13		
	S111C	p	JPW4039		597	598	0.24	+	0.33	34	14
			JPW4042		644	644	0.18	+	**1.49**	15.8	1.5
			JPW4045		634	642	0.01	–	1.07		
			Acrylodan		499	501	0.11	+	**1.61**	4.8	2.3
			Fluorescein		521	521	0.07	–	0.18	2.6	1.9
			NBD		538	542	0.01	+	0.18		
	T44C	p	JPW4039		594	596	0.13	–	0.33		
			JPW4042		634	635	0.06	–	0.30		
			JPW4045		640	636	0.13	–	0.82		
			Acrylodan		499	501	0.01	–	**1.52**		
			Fluorescein		522	522	0.05	–	0.21	0.64	0.38
			NBD		539	536	0.11	–	0.30	0.006	0.005
	W315C	p	JPW4039		594	593	**0.26**	–	0.45	1.00	0.19
			JPW4042		645	640	0.05	–	0.16		
			JPW4045		640	640	0.14	–	0.55	3.2	1.0
			Acrylodan		503	504	0.08	–	0.47	0.13	0.04
			Fluorescein		521	521	0.02	–	0.21		
			NBD		546	546	0.15	–	0.37	0.06	0.02
Glu/Asp BP	A207C	p	JPW4039	glutamate	592	593	0.05	–	0.35		
			JPW4042		635	634	0.20	–	**1.37**		
			JPW4045		637	639	0.15	–	1.19		
			Acrylodan		498	497	**0.26**	+	**1.61**		

(continued)

Table 5. *Continued*

Protein[a]	Mutant	Site[b]	Fluorophore	Ligand	$\lambda_{max,\ apo}$	$\lambda_{max,\ sat}$	ΔI_{std}[c]	Inc/dec[d]	ΔR_{max}[c]	K_d (μM)	Std. error
			Fluorescein		520	502	0.12	–	0.25		
			NBD		529	542	0.05	+	**2.53**	119	11
	A210C	p	JPW4039		593	594	0.08	–	0.26		
			JPW4042		648	645	0.11	–	0.79	0.103	0.054
			JPW4045		647	650	0.09	–	0.71		
			Acrylodan		497	496	0.09	–	0.40		
			Fluorescein		522	522	0.02	–	0.14		
			NBD		543	542	0.02	–	0.30		
	E119C	p	JPW4039		593	594	0.12	+	0.34		
			JPW4045		649	644	0.08	+	**1.73**		
			Acrylodan		498	497	0.11	+	0.65		
			Fluorescein		523	523	0.05	–	0.09		
			NBD		544	544	0.05	–	0.25		
	F126C	a	JPW4039		596	592	0.11	+	0.85		
			JPW4042		642	643	0.01	+	0.40		
			JPW4045		654	643	**0.33**	+	**1.27**	903	94
			Acrylodan		495	482	0.07	+	**2.70**	82	13
			Fluorescein		522	519	0.22	+	**1.73**	1.71 mM	0.13 mM
			NBD		571	572	0.03	+	0.79		
	F131C	a	JPW4039		593	597	0.15	–	0.37	0.151	0.080
			JPW4042		650	643	0.06	–	0.68		
			JPW4045		649	642	0.02	–	0.48		
			Acrylodan		487	492	0.08	–	0.84		
			Fluorescein		522	522	0.05	–	0.13		
			NBD		539	541	0.01	+	0.10		
	F270C	p	JPW4039		596	594	0.01	–	0.11		
			JPW4042		640	645	0.08	+	0.14		
			JPW4045		644	647	0.07	–	0.69		
			Acrylodan		490	492	0.07	–	0.60		
			Fluorescein		523	523	0.04	–	0.21		
			NBD		572	571	0.06	+	0.31		
	G211C	p	JPW4039		594	592	0.01	+	0.12		
			JPW4042		628	631	0.09	+	0.12		
			JPW4045		631	634	0.06	+	0.36		
			Acrylodan		493	492	0.02	–	0.29		
			Fluorescein		522	521	0.03	–	0.18		
			NBD		538	538	0.07	+	0.32		
	K268C	p	Acrylodan		496	497	0.03	–	0.72		
			Fluorescein		522	522	0.06	–	0.18		
	Q123C	p	JPW4039		592	588	0.05	+	0.75		
			JPW4045		640	641	0.00	–	0.88		
			Acrylodan		498	495	0.10	–	0.40		
			Fluorescein		524	522	0.13	–	**2.33**	0.75	0.09
			NBD		544	542	0.01	+	0.53		
	T129C	a	JPW4039		587	584	0.09	+	0.73	0.093	0.015
			JPW4042		649	650	0.06	–	0.68		
			JPW4045		644	648	0.05	–	0.73		
			Acrylodan		484	482	0.04	+	0.52		
			Fluorescein		523	523	0.02	–	0.17		
			NBD		537	538	0.09	+	0.15	0.019	0.011
Fe(III) BP	E203C	p	JPW4039	Fe(III) citrate	599	592	0.09	–	0.37		
			Acrylodan		518	518	**0.41**	–	0.95	138	21
			Fluorescein		523	522	**0.33**	–	0.15	41.9	3.5
			NBD		550	548	**0.31**	–	0.21	221	31
	K202C	p	JPW4039		602	602	0.24	–	0.36	193	29
			Acrylodan		505	503	**0.37**	–	1.17	195	25
			Fluorescein		520	521	**0.30**	–	0.09	195	16
			NBD		542	543	0.23	–	0.14	260	36
	K85C	a	JPW4039		593	591	0.05	–	0.10		
			JPW4042		638	641	0.03	–	0.28		

(continued)

Table 5. *Continued*

Protein[a]	Mutant	Site[b]	Fluorophore	Ligand	$\lambda_{max,\ apo}$	$\lambda_{max,\ sat}$	ΔI_{std}[c]	Inc/dec[d]	ΔR_{max}[c]	K_d (μM)	Std. error
			Acrylodan		503	501	0.05	–	0.41		
			Fluorescein		519	520	0.01	–	0.03		
			NBD		545	543	0.08	–	0.12		
	V287C	a	JPW4039		596	595	0.13	–	0.59		
			JPW4042		596	591	0.06	–	0.24		
			Acrylodan		504	506	0.21	–	0.34	221	35
			Fluorescein		521	520	0.21	–	0.05	92.5	7.5
			NBD		551	552	0.05	–	0.11	0.66	0.27
glucose BP	D257C	a	Acrylodan	glucose	505	509	0.18	–	**1.97**	0.30	0.02
			Fluorescein		523	522	0.07	+	0.41		
			NBD		545	547	**0.72**	–	0.68	1.39	0.01
			Pyrene		401	402	0.06	+	0.98		
	E149C	p	Acrylodan		525	519	**0.60**	+	**2.26**	0.90	0.03
			Fluorescein		527	518	**0.32**	+	**3.63**	253	2
			NBD		549	539	***1.74***	+	***2.46***	2.94	0.12
			Pyrene		385	388	**0.81**	+	**2.60**	20.2	0.3
	E93C	p	Acrylodan		461	462	**0.44**	–	**2.81**	8.74	0.08
			Fluorescein		523	521	0.10	+	0.56	0.77	0.03
			NBD		557	546	**0.53**	+	**3.27**	12.3	0.2
			Pyrene		384	385	0.11	+	0.82		
	H152C	e	Acrylodan		527	524	**0.51**	+	**2.97**	48.1	0.5
			Fluorescein		525	519	**0.40**	+	**2.68**	33.7	0.5
			NBD		546	549	**1.29**	+	1.20	134	1
			Pyrene		408	389	***1.75***	+	***4.63***	79.3	0.4
	L255C	a	Acrylodan		506	509	**0.57**	–	**1.98**	0.494	0.004
			Fluorescein		525	523	0.23	+	**1.49**	0.159	0.009
			NBD		541	548	0.19	+	**1.71**	0.263	0.021
			Pyrene		387	385	**0.90**	+	0.62	0.133	0.022
	N15C	e	Acrylodan		522	524	0.18	–	0.68	0.21	0.01
			Fluorescein		521	522	0.02	+	0.07		
			NBD		544	547	0.04	–	0.82	0.135	0.007
			Pyrene		400	408	**0.51**	+	**2.62**		
	V296C	a	Acrylodan		501	503	0.00	–	0.63		
			Fluorescein		522	522	0.08	–	0.22	0.216	0.006
			NBD		541	543	**0.40**	–	1.06	0.169	0.011
			Pyrene		388	392	0.14	+	**3.40**		
	W183C	e	Acrylodan		483	504	**0.73**	–	**5.57**	5.98 mM	0.03 mM
			Fluorescein		525	521	0.10	+	1.16	17.6 mM	2.4 mM
			NBD		547	546	0.13	–	0.14	318 mM	15 mM
			Pyrene		391	390	0.06	–	0.95		
	Y10C	e	Acrylodan		498	497	0.15	–	1.16	116	3
			Fluorescein		521	521	**0.43**	+	1.22	3.31 mM	0.06 mM
			NBD		540	545	0.03	+	**1.28**		
			Pyrene		388	391	0.19	–	**2.87**		
histidine BP	E167C	p	Acrylodan	histidine	504	506	0.17	+	0.72	0.060	0.003
			Fluorescein		517	518	0.08	–	0.40		
			NBD		539	541	0.05	+	0.42		
			Pyrene		384	384	0.21	+	1.13		
	K229C	p	Acrylodan		526	527	0.02	–	0.41		
			Fluorescein		517	516	0.03	–	0.05		
			NBD		532	536	0.12	+	0.31		
			Pyrene		384	384	0.16	+	0.73		
	V163C	p	JPW4042		659	654	**0.82**	–	**2.44**	0.25	0.02
			Acrylodan		493	500	0.03	+	**2.05**	0.40	0.01
			Fluorescein		520	521	0.12	–	0.10		
			NBD		542	543	0.17	+	**1.32**	2.37	0.15
			Pyrene		384	384	0.08	+	0.78		
	Y230C	p	Acrylodan		523	522	0.02	–	0.18		
			Fluorescein		517	517	0.05	–	0.07		

(continued)

Table 5. *Continued*

Protein[a]	Mutant	Site[b]	Fluorophore	Ligand	$\lambda_{max,\ apo}$	$\lambda_{max,\ sat}$	ΔI_{std}[c]	Inc/dec[d]	ΔR_{max}[c]	K_d (μM)	Std. error
			NBD		535	534	0.09	+	0.20		
			Pyrene		384	384	0.22	+	0.75		
	F231C	p	Acrylodan		524	525	0.01	–	0.56		
			Fluorescein		516	516	0.03	+	0.06		
			NBD		545	542	0.07	+	0.19		
	Y88C	a	Acrylodan		491	493	0.03	–	0.30		
			Fluorescein		518	518	0.04	–	0.06		
			NBD		532	532	0.01	–	0.18		
			Pyrene		384	384	0.15	+	0.44		
maltose BP	D95C	a	JPW4039	maltose	591	593	0.08	–	0.70		
			JPW4042		663	661	0.01	–	0.15		
			JPW4045		650	645	0.08	+	**1.36**	0.30	0.01
			Acrylodan		522	501	0.04	–	**3.31**		
	F92C	a	JPW4039		577	583	**0.43**	–	**1.74**		
			JPW4042		646	646	0.04	–	0.11		
			Acrylodan		495	484	0.16	+	**2.09**		
			Fluorescein		519	518	0.02	+	0.03		
			NBD		531	533	0.09	+	0.27		
	I329C	a	JPW4039		595	594	0.05	–	0.43		
			JPW4042		660	660	0.05	+	0.60		
			JPW4045		652	649	0.04	+	0.55		
			Acrylodan		498	500	0.02	–	0.79		
			Fluorescein		517	518	0.04	+	0.08		
			NBD		522	523	**0.37**	+	**1.33**	0.20	0.02
	S233C	p	JPW4039		577	583	**0.42**	–	**1.73**	145	6
			JPW4042		670	652	**0.87**	–	**4.00**	382	16
			JPW4045		678	657	**0.42**	+	**3.92**	409	22
			Acrylodan		518	519	0.01	–	0.80		
			Fluorescein		519	519	0.17	+	0.10		
			NBD		544	544	**0.76**	+	0.36	9.3	0.3
phosphate BP	A225C	a	JPW4039	phosphate	591	601	**0.36**	+	**2.86**	0.038	0.019
			JPW4042		615	628	**0.30**	–	**1.32**	0.39	0.08
			JPW4045		621	633	0.02	+	0.82		
			Acrylodan		503	502	0.08	–	**1.95**		
			Fluorescein		522	521	0.01	–	0.97	0.20	0.03
			NBD		544	554	**0.81**	–	1.21	0.27	0.03
	N223C	a	Fluorescein		519	519	0.06	+	0.01		
	N226C	a	JPW4039		595	571	**0.26**	+	**2.94**	0.066	0.054
			JPW4042		573	651	**0.29**	+	**2.05**	0.172	0.148
			JPW4045		675	638	**0.53**	+	**3.83**	0.277	0.169
	S164C	p	JPW4039		599	550	***0.91***	–	***3.39***	0.66	0.03
			JPW4042		630	615	**0.33**	–	**1.78**	1.16	0.22
			JPW4045		645	563	**0.27**	–	**2.99**	0.64	0.06
			Acrylodan		505	503	0.05	+	**3.53**	0.22	0.06
			Fluorescein		521	520	0.07	+	0.30	0.17	0.02
			NBD		539	540	0.02	+	0.42		
	S39C	p	JPW4039		597	551	**0.36**	–	**3.15**	0.42	0.06
			JPW4042		623	622	0.01	+	0.15		
			JPW4045		671	647	0.18	–	**4.13**	0.23	0.04
			Acrylodan		520	520	0.10	–	0.80		
			Fluorescein		519	518	0.03	–	0.21		
			NBD		558	559	0.18	+	0.57	0.14	0.04
glutamine BP	N160C	p	Acrylodan	glutamine	529	527	0.11	+	0.43	0.098	0.023
			NBD		546	543	0.09	+	0.71		
			Pyrene		387	387	0.04	–	0.15		
	F221C	p	JPW4042		654	652	0.18	–	0.70		
			Acrylodan		498	498	0.04	–	0.40		
			Fluorescein		518	518	0.02	–	0.10		
			NBD		544	545	0.06	+	0.36	0.0099	0.0034
			NBDE		538	537	0.04	+	0.24		

(continued)

Table 5. *Continued*

Protein[a]	Mutant	Site[b]	Fluorophore	Ligand	$\lambda_{max,\ apo}$	$\lambda_{max,\ sat}$	ΔI_{std}[c]	Inc/dec[d]	ΔR_{max}[c]	K_d (μM)	Std. error
	K219C	p	Acrylodan		494	500	**0.25**	–	**1.34**	0.38	0.03
			NBDE		510	510	0.02	+	0.21		
	L162C	p	Acrylodan		496	501	**0.46**	–	**2.17**	0.17	0.02
			Fluorescein		523	519	0.17	+	**1.80**	0.38	0.06
	W220C	p	Acrylodan		519	518	0.03	+	0.58		
			Fluorescein		518	518	0.01	–	0.03		
			NBD		538	538	0.03	–	0.45		
			NBDE		510	510	0.00	–	0.28		
			Pyrene		386	390	**0.40**	+	**2.86**		
	Y163C	p	Acrylodan		503	502	0.07	+	**2.52**	1.40	0.12
			Fluorescein		518	518	0.04	–	0.04		
			NBD		530	528	0.05	–	0.30		
			Pyrene		385	385	0.01	–	0.07		
	Y86C	a	JPW4042		653	653	0.11	–	0.83	0.338	0.038
			Acrylodan		490	484	**0.41**	–	0.49	0.052	0.003
			NBD		541	538	**0.27**	–	0.25		
			NBDE		541	551	0.12	+	**1.81**		
ribose BP	A234C	a	JPW4039	ribose	598	600	**0.37**	–	**1.29**	1.84	0.40
			JPW4042		668	654	0.06	–	0.99		
			JPW4045		636	578	***0.98***	–	***4.08***	3.76	0.38
			Acrylodan		504	522	0.01	+	1.18		
			Fluorescein		517	517	0.01	–	0.05		
			NBD		546	548	**0.28**	+	**1.63**	0.735	0.057
	D165C	p	JPW4039		589	593	0.13	–	0.36		
			JPW4042		650	652	0.06	–	0.27		
			JPW4045		646	647	0.04	–	0.77		
			Acrylodan		501	500	0.00	–	0.37		
			Fluorescein		522	522	0.03	–	0.37		
	E192C	p	JPW4039		598	598	**0.44**	–	0.34	2.57	0.67
			JPW4042		646	679	***0.99***	–	***4.01***	5.03	0.77
			JPW4045		646	666	***0.89***	–	***2.47***	15.0	0.4
			Acrylodan		516	516	0.04	–	0.27		
			Fluorescein		526	523	0.12	+	**1.31**	11.4	0.8
			NBD		546	540	0.00	+	**1.67**	2.60	0.26
	L236C	a	JPW4039		589	588	0.08	–	0.29		
			JPW4042		646	670	**0.55**	–	**3.58**	0.62	0.22
			JPW4045		646	658	**0.25**	–	**1.70**	1.53	0.41
			Acrylodan		518	518	0.09	–	0.71		
			Fluorescein		520	520	0.02	–	0.29		
			NBD		518	525	0.11	+	**1.96**	0.10	0.05
	L265C	a	JPW4039		600	596	0.01	–	0.11		
			JPW4042		650	654	**0.91**	–	**2.13**	0.26	0.06
			JPW4045		669	663	0.02	–	0.12		
			Acrylodan		500	501	0.20	–	0.70		
			NBD		545	540	0.01	+	0.13		
	T135C	p	JPW4039		606	606	0.02	–	0.03		
			JPW4042		680	674	0.02	+	0.35		
			JPW4045		647	664	***0.89***	–	***2.45***	>1 mM	
			Acrylodan		518	498	**0.31**	+	**6.26**	0.42 mM	0.01 mM
			Fluorescein		526	523	0.18	+	**1.79**	2.09 mM	0.27 mM
			NBD		542	544	0.08	+	0.22		
sulfate BP	L65C	p	JPW4042	sulfate	629	635	**0.40**	–	**1.82**		
			Acrylodan		492	482	**0.39**	+	**2.95**		
			Fluorescein		520	516	**0.39**	+	**1.31**	1.09	0.05
			NBD		522	521	0.02	–	0.61		
			Pyrene		386	385	0.13	+	1.20		
	N70C	p	JPW4042		522	522	0.01	+	0.18		
			Acrylodan		502	502	0.01	–	0.10		
			Fluorescein		517	517	0.01	–	0.01		
			NBD		524	524	0.01	–	0.14		
			Pyrene		386	386	0.01	–	0.13		

(continued)

Table 5. *Continued*

Protein[a]	Mutant	Site[b]	Fluorophore	Ligand	$\lambda_{max,\ apo}$	$\lambda_{max,\ sat}$	ΔI_{std}[c]	Inc/dec[d]	ΔR_{max}[c]	K_d (μM)	Std. error
	Q294C	p	JPW4042		636	630	**0.27**	–	1.17	0.83	0.08
			Acrylodan		500	500	0.04	–	0.13		
			Fluorescein		515	514	0.00	+	0.11		
			NBD		530	530	0.00	+	0.02		
			Pyrene		384	384	0.01	+	0.08		
	R134C	p	JPW4039		522	518	0.08	–	**2.02**	7.5	0.2
			JPW4042		606	608	**0.52**	+	0.96	29.1	1.2
			Acrylodan		493	478	0.18	–	**2.26**	4.17	0.13
			Fluorescein		512	512	0.01	–	0.02	0.323	0.027
			NBD		531	532	**0.58**	–	0.37	22.4	0.5
			Pyrene		382	386	0.15	+	**1.30**		
	W290C	p	JPW4042		612	624	**0.43**	–	0.89	0.336	0.012
			Acrylodan		496	496	0.04	–	0.03		
			Fluorescein		516	515	0.04	+	0.09		
			NBD		538	537	0.06	–	0.11		
			Pyrene		384	384	0.16	+	0.37		
	Y67C	p	Acrylodan		503	502	0.00	–	0.12		
			Fluorescein		515	515	0.01	–	0.04		
			NBD		536	534	0.13	+	0.20		
			Pyrene		383	383	0.02	+	0.48		

[a] All mutants of arabinose BP were in the C64A background; all mutants in Fe(III) BP were in the E57D background.
[b] (a) allosteric, (e) endosteric, (p) peristeric.
[c] Numbers in bold meet the threshold criteria of sensor utility elaborated in the test; underlined numbers indicate excellent absolute intensity or ratiometric sensors; numbers in bold italic are excellent sensors in both parameters.
[d] Inc/dec, increase (+) or decrease (–) in maximum fluorescence intensity upon ligand binding.

Discussion

The success of the fluorescent biosensor design strategy was evaluated by determining the probability of encountering an effectively responding fluorescent conjugate and assessing how the ligand-binding affinities are affected by the fluorophore conjugate.

Assessment of ligand-mediated changes in fluorescence

Summaries of wavelength shift, ΔI_{std}, and ΔR_{max} for all conjugates (n = 320) are presented as histograms in Figure 6A–C. The distribution of wavelength shifts was symmetrical about zero; that is, there was no overall tendency toward either blue or red shifts (Fig. 6A). Of the entire collection of conjugates, 130 show increases and 190 show decreases in fluorescence intensity upon binding. A portion of this skew is due to the finding that addition of Fe(III) citrate to all Fe(III) BP conjugates caused a decrease fluorescence emission. To examine whether this was due to quenching by Fe(III) in solution, Fe(III) citrate was added to conjugates of other bPBPs and the effect on emission intensity was monitored. It was found that Fe(III) citrate quenched fluorescence in all cases but only at concentrations much higher than those that led to the effect in Fe(III) BP. The decrease in fluorescence intensity observed in all conjugates of Fe(III) BP is therefore due to a binding-specific process and may involve relaxation of the excited state via a metal-mediated redox mechanism (Lakowicz 1999). The probability of encountering a conjugate that responds with a particular intensity declines with increasing magnitude of ΔI_{std} (Fig. 6B). The ratiometric response behaves similarly (Fig. 6C).

The two criteria of greatest utility for optical sensing are ΔI_{std} and ΔR_{max}. The collection of bPBP conjugates was categorized by class of steric site, fluorophore, and protein scaffold, then, for each category, quantified according to the fraction with $\Delta I_{std} > 0.25$ and with $\Delta R_{max} > 1.25$. The results (Tables 6 to 8) give an indication of the overall success rate for finding potentially useful fluorescent biosensor conjugates. For the collection of 320 conjugates, about 24% meet the criterion for ΔI_{std} and about 28%, the criterion for ΔR_{max}.

There appears to be a correlation between signaling success rate and the sequence-related family, or cluster (Tam and Saier Jr. 1993), to which a scaffold belongs. The scaffolds having the highest success rates for ΔI_{std} and ΔR_{max} are arabinose BP, glucose BP, ribose BP, and phosphate BP (Table 6). The former three belong to cluster 2, which includes binding proteins for hexoses and pentoses, whereas phosphate BP, along with sulfate BP, belongs to cluster 6, which includes binding proteins for inorganic polyanions. The scaffolds having the lowest success rate were dipeptide BP (cluster 5, peptide and nickel binding) and the cluster 3 (polar amino acid binding) proteins glutamine BP, histidine BP, and Glu/Asp BP.

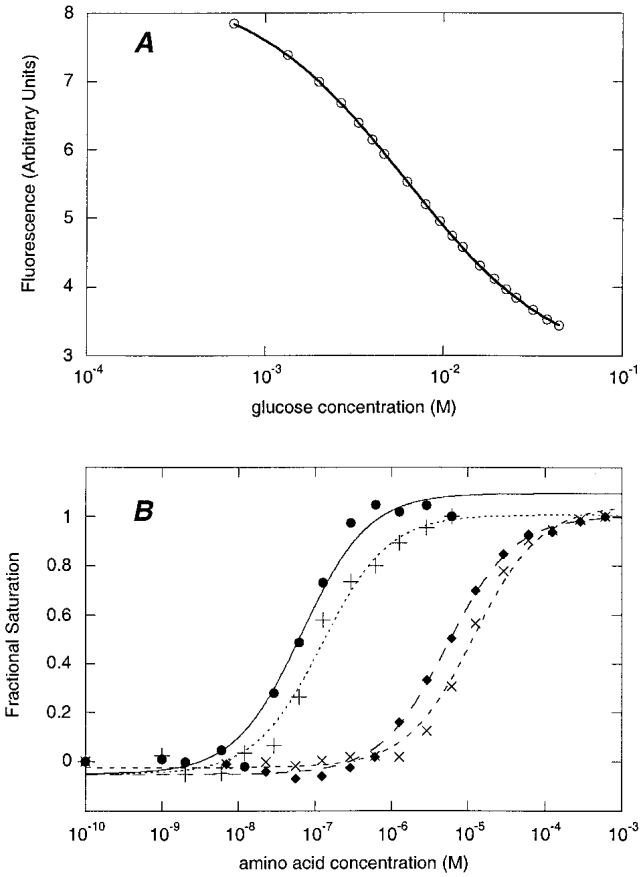

Fig. 5. Fluorimetric titration of glucose BP and glutamate/aspartate BP conjugates. (*A*) Titration of glucose BP W183C-acrylodan with glucose. (*B*) Titration of glutamate/aspartate BP T129C-NBD with amino acids. (•) Glutamic acid; (+) aspartic acid; (◆) asparagine; (×) glutamine. In *A* and *B* the lines shown are the best fit binding isotherms.

Among the three classes of attachment sites the endosteric and allosteric sites have a higher chance of meeting the threshold criteria than peristeric sites (Table 7). Success rates in terms of ΔI_{std} varied according to the environmental sensitivity of the fluorophore, being highest with the styryl and naphthyl dyes JPW4039, JPW4042, and JPW4045. Similarly, higher success rates for ΔR_{max} were associated with JPW4045 and acrylodan (Table 8).

Assessment of changes in ligand-binding affinities

The range of dissociation constants, K_d, extracted from the binding curves for each ligand is shown in Table 9. Because there is a thermodynamic linkage between ligand binding and the interaction of the attached fluorophore with the protein, the fluorophore is expected to change the intrinsic ligand dissociation constant. The change in affinity imparted by the flourophore is expected to be dependent on its location in the protein. The various conjugates exhibit a wide range of affinities (Table 9). We examined the change in affinity, defined as $\log(^{mut}K_d/^{wt}K_d)$, as a function of attachment site classification (endosteric, allosteric, or peristeric) among the 108 conjugates for which dissociation constants were measured and for which the dissociation constant of the unconjugated protein is known (Table 2). The results reveal that the three classes of site have different effects on affinity (Fig. 7). Fluorophore attachment at endosteric sites tends to perturb affinity the most, and uniformly to higher values of K_d than the wild type. Allosteric and peristeric attachment results in K_d values that are either

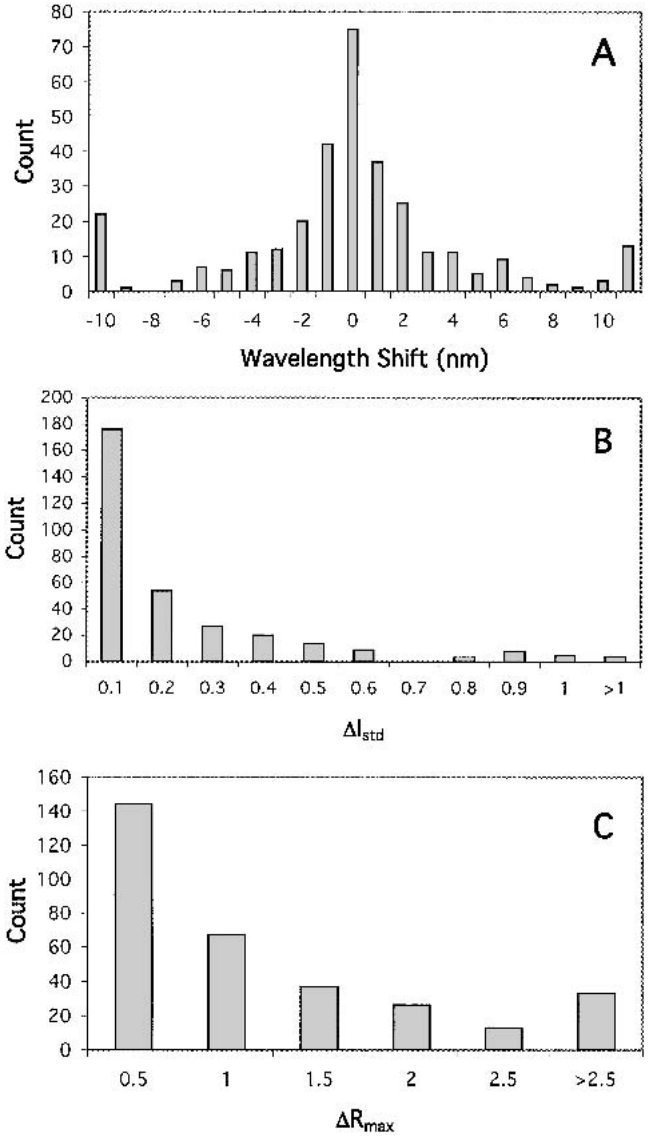

Fig. 6. Occurrence of fluorimetric parameters in the set of 320 fluorescent conjugates. (*A*) Distribution of the shift in wavelength of maximum fluorescent intensity ($^{max}\lambda_{saturated} - {}^{max}\lambda_{apo}$). (*B*) Distribution of the intensity change parameter ΔI_{std}. (*C*) Distribution of the ratiometric change parameter ΔR_{max}. For each parameter, the upper bound of each interval is indicated.

Table 6. *Signaling parameters by binding protein*

Binding protein	Fraction $\Delta I_{std} > 0.25$	Fraction $\Delta R_{max} > 1.25$	*n*
arabinose BP	0.50	0.40	20
glucose BP	0.47	0.50	36
ribose BP	0.32	0.41	34
dipeptide BP	0.08	0.14	36
glutamine BP	0.20	0.24	25
histidine BP	0.04	0.13	24
Glu/Asp BP	0.04	0.15	54
phosphate BP	0.45	0.55	22
sulfate BP	0.23	0.20	30
maltose BP	0.29	0.38	21
Fe(III) BP	0.28	0.00	18
aggregate	0.24	0.28	320

higher or lower than the wild type, with peristeric sites exhibiting the greatest variation in effects. Interestingly, of those conjugates with higher affinity than the wild type (lower K_d), a greater proportion derives from conjugation at allosteric sites. This corroborates detailed studies in maltose BP in which affinity was increased by manipulating the volume of residues in allosteric sites (Marvin and Hellinga 2001b). The differences in effects can be rationalized in terms of the likelihood that a particular conjugate will sterically interfere either directly with ligand binding (endosteric sites, and some peristeric sites), or by influencing the intrinsic equilibrium between the open and closed states (allosteric sites, peristeric sites).

The effect on dissociation constants is determined not only by the attachment site but also by the nature of the attached fluorophore, as illustrated for arabinose BP. Dissociation constants for arabinose of the five cysteine-substitution mutants (all with the C64A mutation), measured by tryptophan fluorescence, are 5.0 μM (F23C), 3.2 μM (L253C), 3.4 μM (D257C), 7.6 μM (L298C), and 1.6 μM (K301C). Thus, the cysteine substitutions slightly perturbed affinity for arabinose (K_d of C64A mutant: 2.2 μM). The largest dependence on the attached fluorophore was found for the L253C mutant, for which K_d values ranged from 0.7 μM (acrylodan) to 775 μM (NBD). Similarly, the K394C mutant of dipeptide BP has affinities for Gly–Leu dipeptide ranging from 6 nM (NBD) to 93 μM (fluorescein). Most mutants did not exhibit such a wide range of fluorophore-dependent ligand affinity. For example, five different fluorophores conjugated to ribose BP E192C have affinities for ribose ranging from 2.6 μM (NBD and JPW4039) to 15 μM (JPW4045).

Table 7. *Signaling parameters by steric site*

Site	Fraction $\Delta I_{std} > 0.25$	Fraction $\Delta R_{max} > 1.25$	*n*
allosteric	0.28	0.32	110
peristeric	0.20	0.15	198
endosteric	0.50	0.50	12
aggregate	0.24	.28	320

Table 8. *Signaling parameters by fluorophore*

Fluorophore	Fraction $\Delta I_{std} > 0.25$	Fraction $\Delta R_{max} > 1.25$	*n*
Acrylodan	0.21	0.38	66
Fluorescein	0.13	0.16	62
NBD	0.25	0.20	61
NBDE	0.00	0.25	4
Pyrene	0.22	0.30	23
JPW4039	0.38	0.28	39
JPW4042	0.32	0.30	37
JPW4045	0.29	0.39	28
aggregate	0.24	0.28	320

Construction of a novel biosensor using sequence information

To demonstrate that designs are not limited to those bPBPs with known structure, we introduced cysteine mutations into a paralog predicted to code for a glutamate/aspartate BP, using histidine and glutamine BPs as the structures to guide locations for likely peristeric and allosteric sites. All of the 10 sites that were tried yielded conjugates that exhibited glutamate- and aspartate-dependent changes in fluorescence. Several sites yielded good or excellent intensiometric or ratiometric sensors. Table 10 shows that the response is specific for both aspartate and glutamate, with 50- to 500-fold weaker affinity for glutamine and asparagine. Other amino acids and sugars did not elicit ligand-mediated changes in fluorescence (not shown).

Bioinformatics offers the promise of discovering new biochemical applications without direct experimentation. In the case of biosensors, individual bacterial genomes may

Table 9. *Range of ligand affinities in bPBP fluorescent conjugates*

bPBP	Ligand	Range of K_d (μM)	*n*
arabinose BP	arabinose	0.46–775	19
glucose BP	glucose	0.13–318000	26
ribose BP	ribose	0.1–2090	14
dipeptide BP	Gly-Leu	0.006–93	21
glutamine BP	glutamine	0.01–1.4	8
histidine BP	histidine	0.06–2.37	4
Glu/Asp BP	glutamate	0.019–1700	9
phosphate BP	phosphate	0.038–1.2	12
sulfate BP	sulfate	0.32–29	8
maltose BP	maltose	0.2–409	6
Fe(III) BP	Fe(III) citrate	0.66–260	10

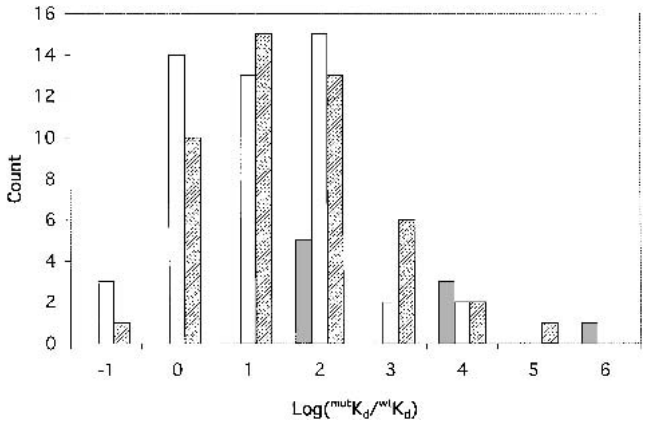

Fig. 7. Occurrence of changes in ligand affinity among the three classes of fluorophore attachment site. (Solid) Endosteric sites; (hatched) peristeric sites; (open) allosteric sites. In the case of arabinose BP, the value for $^{wt}K_d$ is that of the C64A mutant, in which all conjugates were made. Data for dipeptide BP and Fe(III) BP are not included. For the former, the K_d for Gly-Leu dipeptide in the wild type has not been reported. In the case of Fe(III) BP, the K_d of the unconjugated mutant E57D was not determined. For each interval on the x-axis, the upper bound is indicated. For example, the interval labeled "0" contains values of $\log(^{mut}K_d/^{wt}K_d) > -1$ and ≤ 0.

encode scores of bPBPs that bind specific molecules to initiate transport or signal transduction (Blattner et al. 1997; Quentin et al. 1999). Few of these have been characterized, leaving a vast number untapped as scaffolds for potential biosensors. We have demonstrated the feasibility of applying genomic information, combined with structural information from homologous proteins, to construct a biosensor of novel specificity.

Previously, a glutamate/aspartate BP had been purified from *E. coli* (Barash and Halpern 1975; Willis and Furlong 1975) and characterized. Several pieces of evidence suggest that YBEJ corresponds to this protein. First, glutamate/aspartate BP was isolated from periplasmic extracts, consistent with *ybeJ* encoding a protein with a putative periplasmic localization signal sequence. Second, the previously determined molecular mass of glutamate/aspartate BP of 32 kD (Barash and Halpern 1975) or 31 kD (Willis and Furlong 1975) matches the mass of 32.5 kD predicted for the processed *ybeJ* product and the mass of 30 kD found by gel electrophoresis in this study. Third, the amino acid compositions determined previously (Barash and Halpern 1975; Willis and Furlong 1975) are similar to that predicted from the gene sequence, with some deviations likely attributable to inherent inaccuracy in analysis of protein acid hydrolyzates. Finally, the reported K_d values for glutamate (0.8 μM) and aspartate (1.2 μM), as well as the relatively lower affinity for glutamine and asparagine (Willis and Furlong 1975), are similar to those determined here and comparable to the Q123C-fluorescein conjugate (Table 10). Hence, *ybeJ* likely encodes the glutamate/aspartate BP characterized previously.

Effective sensor designs

The utility of a conjugate is determined by the absolute change in signal intensity, the ratiometric change, and the operating concentration range over which the sensor can respond accurately. Of the two observable parameters, ratiometric change is preferable to absolute intensities, because it is independent of probe concentration.

Although we define usable conjugates as having $\Delta I_{std} > 0.25$ and $\Delta R_{max} > 1.25$, "excellent" sensors are defined as having $\Delta I_{std} > 0.9$ and $\Delta R_{max} > 2.5$. The magnitudes of the changes in the excellent sensors are likely to be sufficiently large to permit robust measurements in "real-world" applications in complex fluids such as blood. Based on these criteria there are only 13 excellent absolute intensity-based sensors (4% of total), but 36 excellent ratiometric sensors (11% of total); there are 7 conjugates that are both excellent absolute intensity and excellent ratiometric sensors (Table 5). With the exception of dipeptide BP, Fe(III) BP, and histidine BP, all of the proteins have at least one excellent ratiometric and intensity-based conjugate. Glucose BP has the largest number of excellent conjugates. These conjugates all involve fluorophores known to be particularly environmentally sensitive (acrylodan, NBD, pyrene, and the styryl dyes). The incidence of excellent sensors is evenly distributed between allosteric and peristeric sites. All endosteric sites give rise to excellent sensors.

The dissociation constant of a conjugate determines the operating concentration range over which the sensor can respond accurately. The operating range guaranteed to give <5% error spans concentrations that fall within fivefold of the K_d value (Marvin et al. 1997). If the range required for accurate determination is wider than that span, then a composite biosensor can be constructed using receptors of varying affinities, as has been demonstrated for maltose BP (Marvin et al. 1997). There are three factors affecting the dissociation constant: the nature of the conjugate; the choice of emission bands for a ratiometric sensor (equation 2); and additional mutations. For particular applications these three

Table 10. *Binding specificity and affinity in mutants of glutamate/aspartate BP*

		K_d (μM)			
Mutant	Fluorophore	Glu	Asp	Gln	Asn
Q123C	Fluorescein	0.75	1.8	49	96
F126C	Acrylodan	82	115		
F126C	Fluorescein	1707	2000		
F126C	JPW4045	903	1497		
T129C	NBD	0.019	0.061	12.1	5.4
T129C	JPW4039	0.093	0.035	23	
F131C	JPW4039	0.15			
A207C	NBD	119	454		
A210C	JPW4042	0.10			

factors can be manipulated to construct an appropriate sensor. In the next sections we describe how some of the conjugates might be deployed in real-world applications.

Glucose sensor

Among the analytes applicable to clinical medicine, glucose is one of the most important, particularly with regard to diagnosing and treating diabetes. The normal range of glucose concentration in adult human serum is 4 mM–6 mM (Burtis and Ashwood 1994). The acrylodan conjugate of the endosteric site W183C in glucose BP has an excellent ratiometric response (ΔR_{max} = 5.57) and a dissociation constant of 5.98 mM and is, therefore, a good candidate for detecting glucose fluctuations in the physiological range by ratiometry (Fig. 8A). Furthermore, by adjusting the ratiometric parameters, the observation window is easily extended from 5.0 to 17.4 mM, allowing all clinically relevant ranges to be observed with one sensor (Fig. 8A).

Other sensors for clinical chemistry

Amino acids are also commonly assayed in clinical tests as indicators of disease states. Histidine is an indicator of histidase deficiency (Taylor et al. 1991). The best signaling histidine BP conjugate, V163C-JPW4042, has a K_d of 0.25 μM, below the normal range in serum of about 48–125 μM. However, with sample dilution this conjugate could function effectively. Alternatively, the K_d can be adjusted by mutagenesis as was done for maltose BP (Marvin and Hellinga 2001b) and Fe(III) BP with the E57D mutation. The neuro-excitatory amino acid glutamate has normal serum concentrations of 20–220 μM (Burtis and Ashwood 1994). The best-suited biosensor is glutamate/aspartate BP F126C-acrylodan, which has a K_d of 80 μM and ΔR_{max} of 2.70. Glutamine is often measured in cerebrospinal fluid (Smith and Forman 1994), in which its normal range is 120–360 μM, considerably higher than the K_d (1.4 μM) of the best-signaling glutamine BP conjugate, Y163C-acrylodan. This biosensor could be used for such a purpose by mutagenesis to adjust the K_d, or by sample dilution.

Phosphate concentrations in serum and urine are clinically relevant (Burkhardt et al. 1979). Several phosphate BP conjugates signal well, the best being S39C-JPW4045, and their K_d values are all <2 μM. Inorganic phosphate in serum is typically 1–3 mM (Burtis and Ashwood 1994), requiring adjustment of the K_d or sample dilution for accurate measurements with these sensors.

Maltose concentration is relevant to a deficiency in acid maltase, with the normal plasma concentration about 2 μM (Rozaklis et al. 2002). The best maltose sensors in the present work are maltose BP conjugates S233C-JPW4042 (ΔR_{max} 4.0) and S233C-JPW4045 (ΔR_{max} 3.9), both with similar affinities (K_d ~400 μM). Fluorescent conjugates of maltose BP mutants having affinities in the 2 μM range have been described (Marvin et al. 1997).

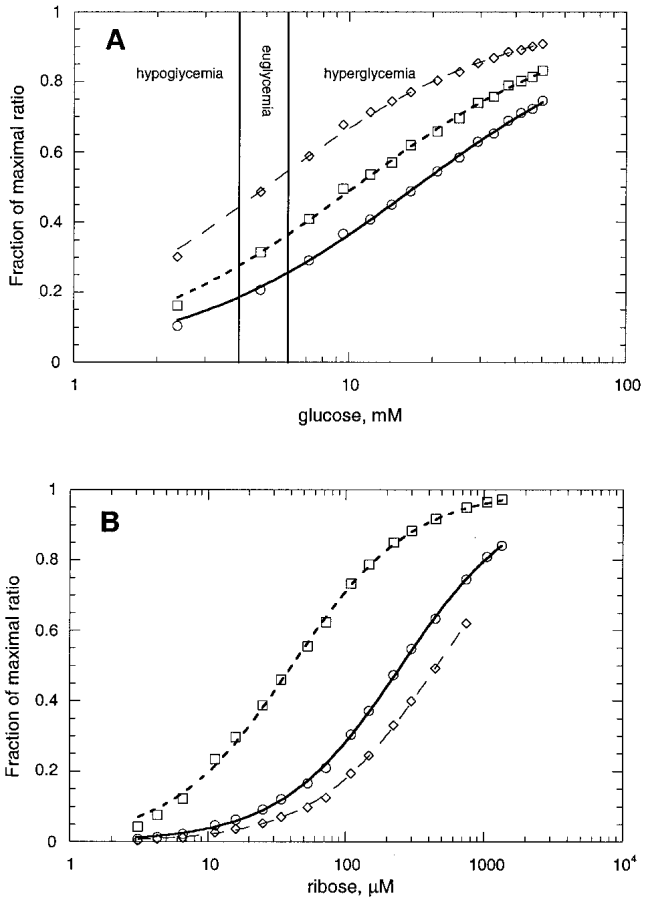

Fig. 8. Ratiometric titration of bBPB fluorophore conjugates using different pairs of emission wavelength bands. (*A*) Glucose BP-W183C conjugated to acrylodan, titrated with glucose at the following ratios of fluorescence emission (wavelengths in nm): (◇) $F_{450–459}/F_{550–559}$ ($^{app}K_d$ = 5.0 mM); (□) $F_{450–459}/F_{486–495}$ ($^{app}K_d$ = 10.4 mM); (○) $F_{472–481}/F_{450–459}$ ($^{app}K_d$ = 17.4 mM). Lines show fit to equation 4. The normal serum glucose range (euglycemia) of 4 mM–6 mM is delimited by vertical lines. (*B*) Ribose BP-T135C conjugated to acrylodan, titrated with ribose at the following ratios of fluorescence emission (wavelengths in nm): (□) $F_{501–510}/F_{450–459}$ ($^{app}K_d$ = 41 μM); (○) $F_{450–459}/F_{501–510}$ ($^{app}K_d$ = 254 μM); (◇) $F_{450–459}/F_{547–556}$ ($^{app}K_d$ = 461 μM).

Industrial and environmental applications

Several bPBP conjugates may function as sensors for industrial and environmental analytes. Arabinose is relevant to improving the efficiency of ethanol production from corn (Deanda et al. 1996). Of the arabinose BP conjugates, the best signalers are K301C-NBD (K_d 31 μM, ΔR_{max} 3.2) and L253C-fluorescein (K_d 48 μM, ΔR_{max} 2.7). Ribose concentration, assayed in foods and beverages (AOAC 1995), could be measured by ribose BP conjugates T135C-acrylodan (K_d 0.4 mM, ΔR_{max} 6.3) and A234C-JPW4045 (K_d 3.8

μM, ΔR_{max} 4.1). Ratiometric sensing of ribose using a single ribose BP derivative is illustrated by the T135C-acrylodan conjugate (Fig. 8B). By varying emission wavelength bands in the fluorescence ratio (equations 4 and 5), the $^{app}K_d$ for ribose can be adjusted over a range from 41 to 146 μM (Fig. 8B). Sulfate concentrations in drinking water are of concern (EPA 1999) and could be analyzed by sulfate BP conjugate R134C-acrylodan (K_d 4 μM, ΔR_{max} 2.3). High concentrations of phosphate are environmentally deleterious and could be monitored using phosphate BP conjugates, as noted above for clinical applications. Iron concentration limits primary productivity in certain regions of the oceans (Martin 1992). Available ferric ion might be determined using a biosensor derived from Fe(III) BP, such as conjugate E203C-acrylodan (K_d 138 μM, ΔI_{std} 0.4).

Conclusions

We have demonstrated that it is possible to construct a large number of diverse sensors using the bPBP superfamily by coupling ligand-mediated hinge-bending motions to changes in fluorescence intensity of conjugated fluorophores by applying relatively straightforward structural design principles. Furthermore, we have shown that the approach is sufficiently robust to construct sensors using homologs whose structure is not known by applying structural homology arguments to position the fluorophores within the sequence. Fluorescent conjugates can be isolated that show large ligand-mediated changes in fluorescence and that respond in the relevant concentration range of various analytes (e.g., glucose).

Although a substantial fraction of conjugates in most bPBPs show large changes in fluorescence emission spectra, many conjugates do not. Within a given bPBP some attachment sites are more effective than others, and within a given attachment site some fluorophores are more effective than others. This points to a need to understand detailed interactions between protein and fluorophore in both the open and closed states. Studies of fluorescence quenching in NBD-conjugated glucose BP (Marvin and Hellinga 1998) showed the absence of large differences in solvent accessibility of the fluorophore between the open and closed states. In NBD-conjgated maltose BP (Gilardi et al. 1997), ligand binding induced differences in spectral properties have been interpreted in terms of altered conformations of the fluorophore. The crystal structure of a fluorophore-conjugate of phosphate BP in the ligand-bound state has been determined and used to rationalize differences in spectral properties in terms of changes in fluorophore mobility attending protein conformational change (Hirshberg et al. 1998). The challenge for future design approaches will be to generate detailed structural models of the fluorophore conjugates to predict sites and choice of fluorophore that optimize physical signal transduction.

Materials and methods

Molecular cloning

PCR was used to amplify wild-type genes for bPBPs from genomic DNA of *E. coli* strain CSH100 (arabinose, dipeptide, histidine, ribose, sulfate, and glutamate/aspartate BP), strain W1485 (glucose and glutamine BP) and strain RU1012 (phosphate BP), or *H. influenzae* strain Rd [Fe(III) BP]. Amplified products were cloned into one of the protein expression vectors pAED4 (Doering 1992), pKK223–3 (Brosius and Holy 1984), or pET vectors (Studier et al. 1990) (Novagen). N-terminal oligonucleotide primers were designed to clone only the processed periplasmic form, deleting the signal sequence. The C-terminal primer was designed to append the sequence Gly-Ser-Gly-$(His)_n$ or Gly-Ser-$(His)_n$, where $n = 5$, 6, or 10. Two tandem stop codons (TAATGA) follow the last His codon. Maltose BP mutants were made in and expressed from plasmid pMAL-c2X (New England BioLabs). *E. coli* strains XL1-BLUE (Stratagene) and DH5α (Hanahan 1983) were used for plasmid construction. Single amino acid substitutions were generated by overlapping PCR mutagenesis (Ho et al. 1989). All clones and mutations were confirmed by nucleotide sequencing. In the case of arabinose BP the single cysteine in the wild-type sequence was replaced by alanine to eliminate the possibility of reporter group conjugation to this thiol (Miller III et al. 1979). Additionally, the sequence of Fe(III) BP was mutated by substitution of Glu57 with Asp to raise the K_d to a concentration range conveniently measured using Fe(III) citrate.

Protein expression

Plasmids were transformed into *E. coli* strain BL21-DE3, grown in nutrient broth overnight at 37°C, then diluted 100-fold into fresh medium and grown further at 37°C or 25°C. Expression was induced by the addition of isopropyl β-D-1-thiogalactopyranoside to 1 mM when the optical density of the culture at 600 nm reached 0.4. After 2–4 h, cells were harvested by centrifugation, resuspended in 20 mM 3-morpholinopropanesulfonic acid (MOPS), 100 mM NaCl at pH 6.9, and stored frozen or lysed immediately for protein purification.

Protein purification

Cells were lysed by sonication or by passage through a French pressure cell. The lysate was treated by adding Polymin P to 0.33% (w/v), chilling on ice for 15 min, then centrifuging to pellet cell debris. The supernatant was loaded on a Ni(II)-charged column of Chelating Sepharose Fast Flow (Amersham Pharmacia Biotech) equilibrated with 20 mM MOPS, 500 mM NaCl, 10 mM imidazole at pH 7.5. The column was washed with loading buffer, then with the same containing 60 mM imidazole, followed by the same with 100 mM imidazole. Finally, protein was eluted with loading buffer containing 400 mM imidazole and was collected in fractions and assessed for purity by gel electrophoresis. All preparations were at least 95% pure by this criterion. Protein-containing fractions were dialyzed exhaustively against buffer (20 mM MOPS, 100 mM NaCl at pH 6.9, or 20 mM NaH_2PO_4, 100 mM NaCl at pH 6.9) or desalted by gel filtration to remove bound ligand.

Fluorophore conjugation to cysteine-substituted bPBPs

Thiol-reactive fluorophores obtained from Molecular Probes (Eugene, OR) were 5-iodoacetamidofluorescein (fluorescein); N-(1-

pyrene) iodoacetamide (pyrene); N,N'-dimethyl-N-(iodoacetyl)-N'-(7-nitrobenz-2-oxa-1,3-diazol-4-yl)ethylenediamide (NBD); N-((2–(iodoacetoxy)ethyl)-N-methyl)amino-7-nitrobenz-2-oxa-1,3-diazole (NBDE); and 6-acryloyl-2-dimethylaminonaphthalene (acrylodan). The styryl and naphthyl dyes JPW4039, JPW4042, and JPW4045 (Fig. 3) were synthesized at the University of Connecticut. All fluorophore conjugation steps were typically carried out at room temperature. To protein at a concentration of 100 μM was added tris-(2-carboxyethyl)phosphine HCl to a fivefold molar excess to reduce intermolecular disulfide bonds. A thiol-reactive fluorophore (20–25 mM in acetonitrile or dimethyl sulfoxide) was added in small aliquots to a fivefold molar excess over protein. Conjugation proceeded in the dark at room temperature for 4 h, or overnight at 4°C. Separation of protein from unreacted fluorophore was achieved by exhaustive dialysis or by size-exclusion chromatography. The efficiency of reporter group attachment was assessed by determination of unreacted thiol with Ellman's reagent (Ellman 1958) or by measuring the ratio of fluorophore to protein from absorbance spectra of the purified conjugate.

Depletion of sulfate and phosphate

Solutions of sulfate BP and phosphate BP and their buffers were treated to decrease the concentration of contaminating sulfate and phosphate, respectively. Sulfate BP buffer (20 mM Tris-HCl, pH 8.0) was passed through the chloride form of Dowex 1X2–100 strongly basic anion-exchange resin. Sulfate BP solutions were treated by dialysis against treated buffer; Dowex resin held in a separate dialysis tube was also included. Phosphate BP solutions and buffer (20 mM MOPS, 100 mM NaCl at pH 6.9) were depleted of phosphate by addition of 7-methylguanosine to 1 mM and dialyzed against bacterial nucleoside phosphorylase (1 unit/mL) (Sigma-Aldrich) partitioned in a separate dialysis tube (Brune et al. 1994).

Fluorimetry

All measurements were conducted with an SLM Aminco-Bowman series 2 fluorimeter, with sample stirring at 25°C. Fluorescence emission spectra were acquired with excitation and emission slit widths of 4 and 8 nm, respectively. Photomultiplier tube potential was maintained between 400 and 800 volts. Protein concentrations were in the range of 50 to 1000 nM. Fluorophore-specific excitation was at the following approximate wavelengths: tryptophan, 290 nm; acrylodan, 390 nm; fluorescein, 485 nm; pyrene, 340 nm; NBD and NBDE, 490 nm; JPW4039, 485 nm; JPW4042, 470 nm; JPW4045, 470 nm.

To measure ligand binding affinity, ligand was serially added to 3 mL of bPBP at a concentration of 50–1000 nM, and emission intensities were recorded. Corrections were made for dilution of the protein and for background signal from buffer. Binding curves were fit to binding isotherms using equation 3 or 4, as appropriate.

Fe(III) BP has a dissociation constant for Fe(III) on the order of 10^{-21} M (Adhikari et al. 1995), hindering accurate fluorescence-based measurements of affinity at nanomolar protein concentrations. Hence, we used Fe(III) citrate (logK = 10.25) (Martell and Smith 1977) as the ligand in a competition assay.

Acknowledgments

Funding for this work was provided by grants from the National Institutes of Health and the Office of Naval Research to H.W.H. Expert technical assistance was contributed by Gregory Shirman and Sara Conrad.

The publication costs of this article were defrayed in part by payment of page charges. This article must therefore be hereby marked "advertisement" in accordance with 18 USC section 1734 solely to indicate this fact.

References

Abouhamad, W.N., Manson, M., Gibson, M.M., and Higgins, C.F. 1991. Peptide transport and chemotaxis in *Escherichia coli* and *Salmonella typhimurium*: Characterization of the dipeptide permease (Dpp) and the dipeptide-binding protein. *Mol. Microbiol.* **5:** 1035–1047.

Adhikari, P., Kirby, S.D., Nowalk, A.J., Veraldi, K.L., Schryvers, A.B., and Mietzner, T.A. 1995. Biochemical characterization of a *Haemophilus influenzae* periplasmic iron transport operon. *J. Biol. Chem.* **270:** 25142–25149.

Anraku, Y. 1968. Transport of sugars and amino acids in bacteria. I. Purification and specificity of the galactose- and leucine-binding proteins. *J. Biol. Chem.* **243:** 3116–3122.

AOAC. 1995. *Official methods of analysis of AOAC International*, 16th ed. AOAC International, Arlington, VA.

APHA. 1992. *Standard methods for the examination of water and wastewater*, 18th ed. American Public Health Association, Washington, D.C.

Barash, H. and Halpern, Y.S. 1975. Purification and properties of glutamate binding protein from the periplasmic space of *Escherichia coli* K-12. *Biochim. Biophys. Acta* **386:** 168–180.

Benson, D.E., Conrad, D.W., de Lorimier, R.M., Trammell, S.A., and Hellinga, H.W. 2001. Design of bioelectronic interfaces by exploiting hinge-bending motions in proteins. *Science* **293:** 1641–1644.

Berman, H.M., Westbrook, J., Feng, Z., Gilliland, G., Bhat, T.N., Weissig, H., Shindyalov, I.N., and Bourne, P.E. 2000. The Protein Data Bank. *Nucleic Acids Res.* **28:** 235–242.

Bjorkman, A.J. and Mowbray, S.L. 1998. Multiple open forms of ribose-binding protein trace the path of its conformational change. *J. Mol. Biol.* **279:** 651–664.

Blattner, F.R., Plunkett, G., 3rd, Bloch, C.A., Perna, N.T., Burland, V., Riley, M., Collado-Vides, J., Glasner, J.D., Rode, C.K., Mayhew, G.F., et al. 1997. The complete genome sequence of *Escherichia coli* K-12. *Science* **277:** 1453–1474.

Brosius, J. and Holy, A. 1984. Regulation of ribosomal RNA promoters with a synthetic lac operator. *Proc. Natl. Acad. Sci.* **81:** 6929–6933.

Brune, M., Hunter, J.L., Corrie, J.E., and Webb, M.R. 1994. Direct, real-time measurement of rapid inorganic phosphate release using a novel fluorescent probe and its application to actomyosin subfragment 1 ATPase. *Biochemistry* **33:** 8262–8271.

Bruns, C.M., Nowalk, A.J., Arvai, A.S., McTigue, M.A., Vaughan, K.G., Mietzner, T.A., and McRee, D.E. 1997. Structure of *Haemophilus influenzae* Fe(+3)-binding protein reveals convergent evolution within a superfamily. *Nat. Struct. Biol.* **4:** 919–924.

Bruns, C.M., Anderson, D.S., Vaughan, K.G., Williams, P.A., Nowalk, A.J., McRee, D.E., and Mietzner, T.A. 2001. Crystallographic and biochemical analyses of the metal-free *Haemophilus influenzae* Fe3+-binding protein. *Biochemistry* **40:** 15631–15637.

Burkhardt, R.T., Sheiko, M.C., and Batsakis, J.G. 1979. Clinical laboratory estimations of serum and urinary phosphate. *Am. J. Clin. Pathol.* **72:** 326–329.

Burrin, J.M. and Price, C.P. 1985. Measurement of blood glucose. *Ann. Clin. Biochem.* **22:** 327–342.

Burtis, C.A. and Ashwood, E.A. 1994. *Teitz textbook of clinical chemistry*, 2nd ed. W.B. Saunders Co., Philadelphia.

Clark, A.F., Gerken, T.A., and Hogg, R.W. 1982. Proton nuclear magnetic resonance spectroscopy and ligand binding dynamics of the *Escherichia coli* L-arabinose binding protein. *Biochemistry* **21:** 2227–2233.

Dattelbaum, J.D. and Lakowicz, J.R. 2001. Optical determination of glutamine using a genetically engineered protein. *Anal. Biochem.* **291:** 89–95.

Deanda, K., Zhang, M., Eddy, C., and Picataggio, S. 1996. Development of an arabinose-fermenting *Zymomonas mobilis* strain by metabolic pathway engineering. *Appl. Environ. Microbiol.* **62:** 4465–4470.

Doering, D.S. 1992. 'Functional and structural studies of a small f-actin binding domain.' Ph.D. thesis, Massachusetts Institute of Technology.

Dunten, P. and Mowbray, S.L. 1995. Crystal structure of the dipeptide binding protein from *Escherichia coli* involved in active transport and chemotaxis. *Protein Sci.* **4:** 2327–2334.

Duplay, P., Bedouelle, H., Fowler, A., Zabin, I., Saurin, W., and Hofnung, M. 1984. Sequences of the malE gene and of its product, the maltose-binding protein of *Escherichia coli* K12. *J. Biol. Chem.* **259:** 10606–10613.

Ellman, G.L. 1958. A colorimetric method for determining low concentrations of mercaptans. *Arch. Biochem. Biophys.* **74:** 443–450.

EPA. 1999. Health effects from exposure to high levels of sulfate in drinking water study. Publication No. 815R99001 (pp. 1–25). U.S. Environmental Protection Agency, Office of Drinking Water and Ground Water, Washington, DC.

Gilardi, G., Zhou, L.Q., Hibbert, L., and Cass, A.E. 1994. Engineering the maltose binding protein for reagentless fluorescence sensing. *Anal. Chem.* **66:** 3840–3847.

Gilardi, G., Mei, G., Rosato, N., Agro, A.F., and Cass, A.E.G. 1997. Spectroscopic properties of an engineered maltose binding protein. *Prot. Eng.* **10:** 479–486.

Groarke, J.M., Mahoney, W.C., Hope, J.N., Furlong, C.E., Robb, F.T., Zalkin, H., and Hermodson, M.A. 1983. The amino acid sequence of D-ribose-binding protein from *Escherichia coli* K12. *J. Biol. Chem.* **258:** 12952–12956.

Guyer, C.A., Morgan, D.G., and Staros, J.V. 1986. Binding specificity of the periplasmic oligopeptide-binding protein from *Escherichia coli*. *J. Bacteriol.* **168:** 775–779.

Hall, E.E.H. 1991. *Biosensors*. Prentice-Hall, Englewood Cliffs, NJ.

Hanahan, D. 1983. Studies on transformation of *Escherichia coli* with plasmids. *J. Mol. Biol.* **166:** 557–580.

He, J.J. and Quiocho, F.A. 1993. Dominant role of local dipoles in stabilizing uncompensated charges on a sulfate sequestered in a periplasmic active transport protein. *Protein Sci.* **2:** 1643–1647.

Hellinga, H.W. and Evans, P.R. 1985. Nucleotide sequence and high-level expression of the major *Escherichia coli* phosphofructokinase. *Eur. J. Biochem.* **149:** 363–373.

Hellinga, H.W. and Marvin, J.S. 1998. Protein engineering and the development of generic biosensors. *Trends Biotech.* **16:** 183–189.

Hellinga, H.W. and Richards, F.M. 1991. Construction of new ligand binding sites in proteins of known structure. I. Computer-aided modeling of sites with pre-defined geometry. *J. Mol. Biol.* **222:** 763–785.

Hirshberg, M., Henrick, K., Haire, L.L., Vasisht, N., Brune, M., Corrie, J.E., and Webb, M.R. 1998. Crystal structure of phosphate binding protein labeled with a coumarin fluorophore, a probe for inorganic phosphate. *Biochemistry* **37:** 10381–10385.

Ho, S.N., Hunt, H.D., Horton, R.M., Pullen, J.K., and Pease, L.R. 1989. Site-directed mutagenesis by overlap extension using the polymerase chain reaction. *Gene* **77:** 51–59.

Hochuli, E., Dobeli, H., and Schacher, A. 1987. New metal chelate adsorbent selective for proteins and peptides containing neighbouring histidine residues. *J. Chromatogr. A* **411:** 177–184.

Hsiao, C.D., Sun, Y.J., Rose, J., and Wang, B.C. 1996. The crystal structure of glutamine-binding protein from *Escherichia coli*. *J. Mol. Biol.* **262:** 225–242.

Jacobson, B.L. and Quiocho, F.A. 1988. Sulfate-binding protein dislikes protonated oxyacids. A molecular explanation. *J. Mol. Biol.* **204:** 783–787.

Kraulis, P.J. 1991. MOLSCRIPT: A program to produce both detailed and schematic plots of protein structures. *J. Appl. Crystallogr.* **24:** 946–950.

Lakowicz, J.R. 1999. *Principles of fluorescence spectroscopy*, 2nd ed., p. 698. Kluwer Academic Press, New York.

Ledvina, P.S., Yao, N., Choudhary, A., and Quiocho, F.A. 1996. Negative electrostatic surface potential of protein sites specific for anionic ligands. *Proc. Natl. Acad. Sci.* **93:** 6786–6791.

Luecke, H. and Quiocho, F.A. 1990. High specificity of a phosphate transport protein determined by hydrogen bonds. *Nature* **347:** 402–406.

Magota, K., Otsuji, N., Miki, T., Horiuchi, T., Tsunasawa, S., Kondo, J., Sakiyama, F., Amemura, M., Morita, T., Shinagawa, H., et al. 1984. Nucleotide sequence of the phoS gene, the structural gene for the phosphate-binding protein of *Escherichia coli*. *J. Bacteriol.* **157:** 909–917.

Martell, A.E. and Smith, R.M. 1977. *Critical stability constants*. Plenum Press, New York.

Martin, J.H. 1992. Iron as a limiting factor. In *Primary productivity and biogeochemical cycles in the sea* (eds. P.G. Falkowski and A. Woodhead), pp. 123–137. Plenum Press, New York.

Marvin, J.S. and Hellinga, H.W. 1998. Engineering biosensors by introducing fluorescent allosteric signal transducers — construction of a novel glucose sensor. *J. Am. Chem. Soc.* **120:** 7–11.

———. 2001a. Conversion of maltose-binding protein into a zinc biosensor by computational design. *Proc. Natl. Acad. Sci.* **98:** 4955–4960.

———. 2001b. Manipulation of ligand binding affinity by exploitation of conformational coupling. *Nat. Struct. Biol.* **8:** 795–798.

Marvin, J.S., Corcoran, E.E., Hattangadi, N.A., Zhang, J.V., Gere, S.A., and Hellinga, H.W. 1997. The rational design of allosteric interactions in a monomeric protein and its applications to the construction of biosensors. *Proc. Natl. Acad. Sci.* **94:** 4366–4371.

Meadows, D. 1996. Recent developments with biosensing technology and applications in the pharmaceutical industry. *Adv. Drug Deliv. Rev.* **21:** 177–189.

Medveczky, N. and Rosenberg, H. 1969. The binding and release of phosphate by a protein isolated from *Escherichia coli*. *Biochim. Biophys. Acta* **192:** 369–371.

Miller III, D.M., Newcomer, M.E., and Quiocho, F.A. 1979. The thiol group of the L-arabinose-binding protein. Chromophoric labeling and chemical identification of the sugar-binding site. *J. Biol. Chem.* **254:** 7521–7528.

Miller III, D.M., Olson, J.S., Pflugrath, J.W., and Quiocho, F.A. 1983. Rates of ligand binding to periplasmic proteins involved in bacterial transport and chemotaxis. *J. Biol. Chem.* **258:** 13665–13672.

Mowbray, S.L. and Cole, L.B. 1992. 1.7 Å X-ray structure of the periplasmic ribose receptor from *Escherichia coli*. *J. Mol. Biol.* **225:** 155–175.

Nelson, P.V., Carey, W.F., and Pollard, A.C. 1977. A micro-radiochemical assay for α-1,4-glucosidase and its use in the assessment of type II glycogenosis (Pompe's disease). *Clin. Chim. Acta* **77:** 337–342.

Nickitenko, A.V., Trakhanov, S., and Quiocho, F.A. 1995. 2 Å resolution structure of DppA, a periplasmic dipeptide transport/chemosensory receptor. *Biochemistry* **34:** 16585–16595.

Nohno, T., Saito, T., and Hong, J.S. 1986. Cloning and complete nucleotide sequence of the *Escherichia coli* glutamine permease operon (glnHPQ). *Molec. Gen. Genet.* **205:** 260–269.

Oh, B.H., Kang, C.H., De, B.H., Kim, S.H., Nikaido, K., Joshi, A.K., and Ames, G.F. 1994. The bacterial periplasmic histidine-binding protein. Structure/function analysis of the ligand-binding site and comparison with related proteins. *J. Biol. Chem.* **269:** 4135–4143.

Pellegrini, M., Marcotte, E.M., Thompson, M.J., Eisenberg, D., and Yeates, T.O. 1999. Assigning protein functions by comparative genome analysis: Protein phylogenetic profiles. *Proc. Natl. Acad. Sci.* **96:** 4285–4288.

Pflugrath, J.W. and Quiocho, F.A. 1985. Sulphate sequestered in the sulphate-binding protein of *Salmonella typhimurium* is bound solely by hydrogen bonds. *Nature* **314:** 257–260.

Quentin, Y., Fichant, G., and Denizot, F. 1999. Inventory, assembly and analysis of *Bacillus subtilis* ABC transport systems. *J. Mol. Biol.* **287:** 467–484.

Quiocho, F.A. and Vyas, N.K. 1984. Novel stereospecificity of the L-arabinose-binding protein. *Nature* **310:** 381–386.

Quiocho, F.A. and Ledvina, P.S. 1996. Atomic structure and specificity of bacterial periplasmic receptors for active transport and chemotaxis: Variation of common themes. *Molec. Microbiol.* **20:** 17–25.

Quiocho, F.A., Spurlino, J.C., and Rodseth, L.E. 1997. Extensive features of tight oligosaccharide binding revealed in high-resolution structures of the maltodextrin transport/chemosensory receptor. *Structure* **5:** 997–1015.

Rozaklis, T., Ramsay, S.L., Whitfield, P.D., Ranieri, E., Hopwood, J.J., and Meikle, P.J. 2002. Determination of oligosaccharides in Pompe disease by electrospray ionization tandem mass spectrometry. *Clin. Chem.* **48:** 131–139.

Salins, L.L., Ware, R.A., Ensor, C.M., and Daunert, S. 2001. A novel reagentless sensing system for measuring glucose based on the galactose/glucose-binding protein. *Anal. Biochem.* **294:** 19–26.

Sanders, J.D., Cope, L.D., and Hansen, E.J. 1994. Identification of a locus involved in the utilization of iron by *Haemophilus influenzae*. *Infect. Immun.* **62:** 4515–4525.

Scheller, F.W., Wollenberger, U., Warsinke, A., and Lisdat, F. 2001. Research and development in biosensors. *Curr. Opin. Biotech.* **12:** 35–40.

Scholle, A., Vreemann, J., Blank, V., Nold, A., Boos, W., and Manson, M.D. 1987. Sequence of the mglB gene from *Escherichia coli* K12: Comparison of wild-type and mutant galactose chemoreceptors. *Mol. Gen. Genet.* **208:** 247–253.

Schwartz, M., Kellermann, O., Szmelcman, S., and Hazelbauer, G.L. 1976. Further studies on the binding of maltose to the maltose-binding protein of *Escherichia coli*. *Eur. J. Biochem.* **71:** 167–170.

Scripture, J.B., Voelker, C., Miller, S., O'Donnell, R.T., Polgar, L., Rade, J., Horazdovsky, B.F., and Hogg, R.W. 1987. High-affinity L-arabinose transport operon. Nucleotide sequence and analysis of gene products. *J. Mol. Biol.* **197:** 37–46.

Sharff, A.J., Rodseth, L.E., Spurlino, J.C., and Quiocho, F.A. 1992. Crystallographic evidence of a large ligand-induced hinge-twist motion between the

two domains of the maltodextrin binding protein involved in active transport and chemotaxis. *Biochemistry* **31:** 10657–10663.

Smith, M.W., Tyreman, D.R., Payne, G.M., Marshall, N.J., and Payne, J.W. 1999. Substrate specificity of the periplasmic dipeptide-binding protein from *Escherichia coli*: Experimental basis for the design of peptide prodrugs. *Microbiology* **145:** 2891–2901.

Smith, S.V. and Forman, D.T. 1994. Laboratory analysis of cerebrospinal fluid. *Clin. Lab. Sci.* **7:** 32–38.

Spurlino, J.C., Lu, G.Y., and Quiocho, F.A. 1991. The 2.3-Å resolution structure of the maltose- or maltodextrin-binding protein, a primary receptor of bacterial active transport and chemotaxis. *J. Biol. Chem.* **266:** 5202–5219.

Studier, F.W., Rosenberg, A.H., Dunn, J.J., and Dubendorff, J.W. 1990. Use of T7 RNA polymerase to direct expression of cloned genes. *Methods Enzymol.* **185:** 60–89.

Sun, Y.-J., Rose, J., Wang, B.-C., and Hsiao, C.-D. 1998. The structure of glutamine-binding protein complexed with glutamine at 1.94 Å resolution: Comparisons with other amino acid binding proteins. *J. Mol. Biol.* **278:** 219–229.

Tam, R. and Saier, Jr., M.H. 1993. Structural, functional, and evolutionary relationships among extracellular solute-binding receptors of bacteria. *Microbiol. Rev.* **57:** 320–346.

Taylor, R.G., Levy, H.L., and McInnes, R.R. 1991. Histidase and histidinemia. Clinical and molecular considerations. *Molec. Biol. Med.* **8:** 101–116.

Thompson, J.D., Higgins, D.G., and Gibson, T.J. 1994. CLUSTAL W: Improving the sensitivity of progressive multiple sequence alignment through sequence weighting, position-specific gap penalties and weight matrix choice. *Nucleic Acids Res.* **22:** 4673–4680.

Tolosa, L., Gryczynski, I., Eichhorn, L.R., Dattelbaum, J.D., Castellano, F.N., Rao, G., and Lakowicz, J.R. 1999. Glucose sensor for low-cost lifetime-based sensing using a genetically engineered protein. *Anal. Biochem.* **267:** 114–120.

von Heijne, G. 1986. A new method for predicting signal sequence cleavage sites. *Nucleic Acids Res.* **14:** 4683–4690.

Vyas, M.N., Vyas, N.K., and Quiocho, F.A. 1994. Crystallographic analysis of the epimeric and anomeric specificity of the periplasmic transport/chemosensory protein receptor for D-glucose and D-galactose. *Biochemistry* **33:** 4762–4768.

Vyas, N.K., Vyas, M.N., and Quiocho, F.A. 1988. Sugar and signal-transducer binding sites of the *Escherichia coli* galactose chemoreceptor protein. *Science* **242:** 1290–1295.

Weiner, J.H., Furlong, C.E., and Heppel, L.A. 1971. A binding protein for L-glutamine and its relation to active transport in *E. coli. Arch. Biochem. Biophys.* **142:** 715–717.

Willis, R.C. and Furlong, C.E. 1974. Purification and properties of a ribose-binding protein from *Escherichia coli. J. Biol. Chem.* **249:** 6926–6929.

———. 1975. Purification and properties of a periplasmic glutamate-aspartate binding protein from *Escherichia coli* K12 strain W3092. *J. Biol. Chem.* **250:** 2574–2580.

Yao, N., Trakhanov, S., and Quiocho, F.A. 1994. Refined 1.89-Å structure of the histidine-binding protein complexed with histidine and its relationship with many other active transport/chemosensory proteins. *Biochemistry* **33:** 4769–4779.